Flammability reduction in a pressurised water electrolyser based on a thin polymer electrolyte membrane through a Pt-alloy catalytic approach

Nicola Briguglio[a], Stefania Siracusano[a], Giuseppe Bonura[a],

David Sebastián[a,b] and Antonino S. Aricò[a,*]

[a]*CNR-ITAE Institute of Advanced Energy Technologies, National Research Council*

Via Salita S. Lucia sopra Contesse 5, 98126 Messina, Italy

[b]*Instituto de Carboquímica, CSIC. Miguel Luesma Castán 4, 50018 Zaragoza, Spain*

*Corresponding author. Tel.: +39 090 624237; fax: +39 090 624247. E-mail address: arico@itae.cnr.it

ABSTRACT

Various Pt-based materials (unsupported Pt, PtRu, PtCo) were investigated as catalysts for recombining hydrogen and oxygen back into water. The recombination performance correlated well with the surface Pt metallic state. Alloying cobalt to platinum was observed to produce an electron transfer favouring the occurrence of a large fraction of the Pt metallic state on the catalyst surface. Unsupported PtCo showed both excellent recombination performance and dynamic behaviour. In a packed bed catalytic reactor, when hydrogen was fed at 4% vol. in the oxygen stream (flammability limit), 99.5% of the total H_2 content was immediately converted to water in the presence of PtCo thus avoiding safety issues. The PtCo catalyst was thus integrated in the anode of the membrane-electrode assembly of a polymer electrolyte membrane electrolysis cell. This catalyst showed good capability to reduce the concentration of hydrogen in the oxygen stream under differential pressure operation (1-20 bar), in the presence of a thin (90 µm) Aquivion® membrane. The modified system showed lower hydrogen concentration in the oxygen flow than electrolysis cells based on state-of-the-art thick polymer electrolyte membranes and allowed to expand the minimum current density load down to 0.15 A cm^{-2}. The electrolysis cell equipped with a dual layer PtCo/IrRuOx oxidation catalyst achieved a high operating current density (3 A cm^{-2}) as requested to decrease the system capital costs, under high efficiency conditions (about 77% efficiency at 55°C and 20 bar). Moreover, the electrolysis system showed reduced probability to reach the flammability limit under both high differential pressure (20 bar) and partial load operation (5%), as needed to properly address grid-balancing service.

Keywords: Recombination catalyst; Polymer electrolyte membrane electrolysis; PtCo catalyst; Hydrogen; Flammability.

1. Introduction

The main challenges to overcome for an effective, wide-scale, utilisation of hydrogen as energy carrier [1-4], regard both technical bottlenecks and an optimization of the energy cycle [5-7] from renewable energy sources to end use via hydrogen generation, storage, transport, conversion and consumption [5]. Technical problems are primarily dealing with the storage of hydrogen at high volumetric energy density, using low-energy consumption and cost-effective technologies characterised by intrinsic safety [8-14]. Next generation water electrolysers are expected to operate at high pressure to reduce the efficiency losses in the gas post-compression step while offering proper dynamic behaviour in terms of rapid response and partial load operation [8]. Generally, most of the present pressurised polymer electrolyte (PEM) electrolysers cannot operate at a partial load below 20% because of the excessive concentration of hydrogen in the oxygen stream at the anode at low current densities [8,14]. The flammability limit of the H_2 concentration in O_2 is 4% vol. [15] but for safety reasons the systems are shutdown when this concentration exceeds 2-3% vol. [14].

Specific improvements of PEM electrolysers are required especially in terms of significant increase in current density, resulting in the proportional decrease in capital costs, whilst maintaining cutting edge efficiency in combination with a material use minimisation approach [16,17]. This regards a reduced membrane thickness whilst keeping low the gas crossover and reducing the precious metal loading. For a PEM electrolyser operating at high current density, the role of the membrane is dominant in determining voltage efficiency and reaction rate [8,18]. At high current density, the proton transport inside the membrane causes the largest contribution to the overall differential resistance [19,20]. On the contrary, the polarisation resistance, for both anode and cathode processes decreases significantly when the overpotential is increased [19,20]. Advanced PEM electrolysis systems show that, at 3 A cm^{-2}, ohmic losses, mainly caused by the membrane, contribute to about 85% or more of the overall differential resistance [19].

Ohmic losses at high current density decrease proportionally with the decrease of the membrane thickness thus allowing the achievement of much higher current densities at the same voltage efficiency [21]. However, a significant reduction of the membrane thickness will also produce a proportional increase of the gas crossover especially under high differential pressure

operation (pressurised hydrogen and non-pressurised oxygen) causing significant loss of faradaic efficiency beside the occurrence of safety issues and the impossibility to operate under low partial load [22,24]. These are significant restrictions in term of system reliability and dynamic characteristics. After several decades of development, it seems that a further improvement of the proton conductivity of PFSA membranes is hard to achieve in the next years [25-26]. Thus, the achievement of high current densities, as required to reduce the capital costs of PEM electrolysis systems, passes through a necessary reduction of the membrane thickness.

This strategy was already adopted in automotive PEM fuel cells [25]. However, in the fuel cell automotive sector, the use of air blowers requires operation at very low pressure. Thus, for PEM fuel cells operating at ambient pressure, the use of membranes with a thickness of 10-20 μm does not represent an issue in terms of gas crossover and fuel utilisation [25]. This is instead a relevant drawback when a differential pressure of about 20-30 bars is applied between the cathode and anode compartments in PEM electrolysers. In this case, the industry standard is a Nafion 117 membrane with a thickness of 170 μm, in dry form, offering proper protection against gas crossover [22-24].

A decrease of the membrane thickness from 170 to 90 μm (about one-half) would produce a significant decrease of the ohmic drop with a corresponding large increase of reaction rate at a similar voltage efficiency. However, the corresponding increase of hydrogen concentration in the oxygen stream caused by the thinner membrane needs to be minimised. In principle, a one percent loss of faradaic efficiency does not represent a significant drawback if the hydrogen production rate is increased significantly (e.g. twice or more) allowing for a corresponding decrease of the capital costs of the entire system. Instead, a one percent increase of the hydrogen concentration in the oxygen stream would be dramatic for the electrolyser safety characteristics and for the possibility to operate under partial load [15, 22-24, 27-28].

The conventional electrocatalysts used at the anode of a PEM electrolyser are mainly based on Ir metal, which is oxidised on the surface during operation [29], IrO_2 and IrRuOx [30-36]. Unfortunately, these oxidised catalysts are not efficient for molecular hydrogen oxidation [37]. Thus, permeated hydrogen is realesed into the outlet anodic stream. Generally, a PEM electrolyser is equipped with an external catalytic gas recombiner (e.g. a Pt/Al_2O_3 bed) to promote H_2/O_2 recombination in the gas phase, especially to reduce the oxygen contamination level in the produced hydrogen gas [22,28,39]. However, these purification systems are allocated outside the

PEM electrolysis stack for technical reasons. Their use allows essentially a purification of the produced gases but it does not allow improving the internal safety of the stack device.

Based on these considerations, the approach used in this work was to integrate a thin layer of a hydrogen oxidation catalyst in the membrane-electrode assembly, between the membrane and the IrRuOx anode catalyst layer, in order to decrease the concentration of hydrogen in the oxygen stream well below the safety limit. This concept was demonstrated in the presence of a thin (90 µm) PFSA membrane, in a wide range of operating current densities (from 0.3 to 3 A cm^{-2}) and differential pressures (up to 20 bar).

The approach of using a hydrogen oxidation catalyst at the anode can be also employed in combination to other strategies involving membrane modifications [40-44]. As an example, the use of Pt nanoparticles inside the membrane, firstly used to promote internal humidification in fuel cells, can provide a useful internal recombination route for the permeated hydrogen and oxygen gases [45]. However, this strategy requires a recast procedure for membrane production [45]. Similarly, the casting method is also used when specific fillers are added into the membrane to increase the tortuosity factor for gas permeation [41]. On the other hand, an excellent mechanical strength is required for the polymer electrolyte membrane in pressurised electrolysers applications. Thus, extruded membranes are usually employed. The present catalytic approach does not require any membrane modification if low gas permeation and proper faradaic efficiency are guaranteed the polymeric electrolyte separator. Moreover, the approach here developed appears to be simpler than using a Pt electrode layer in between two membrane layers [46].

Thus, the oxidation catalyst here developed is integrated into the membrane-electrode assembly (MEA) to favour the oxidation to protons of the hydrogen permeated at the anode. The formed protons back diffuse to the cathode according to the electroosmotic drag where these are reduced again to hydrogen. This causes a parasitic process that just produces a small decrease of faradaic efficiency; the overall loss of faradaic efficiency is less than 1 % for reasonably thin PFSA membranes of about 90 µm thickness. However, as mentioned above, the limited loss of faradaic efficiency is largely compensated by a significant increase of the hydrogen production rate that is favoured by the use of thinner membranes.

Unfortunately, hydrogen oxidation catalysts based on bare Pt are easily oxidised on the surface to Pt-oxide during operation at the anode of an electrolysis cell [47]. This causes a

decrease of the oxidation activity. Such drawback also affects the Pt layer usually coated onto the Ti-foam current collector [41].

In this work, a highly dispersed unsupported Pt-alloy, with low propensity to form Pt oxides, was used at the anode side of an electrolysis cell. This additional catalytic layer is confined between the perfluorosulfonic membrane and the IrRuOx anode catalyst. Electro-catalytic tests at high differential pressure were restricted to the most promising Pt-based formulation down-selected from ex-situ catalytic tests [38, 39]. The catalyst screening process was carried out through gas-phase catalytic tests in a packed bed reactor allowing to rapidly identifying the properties for H_2-O_2 recombination back into water.

In previous works, we have shown a significant role played by a transition metal in a Pt alloy for the removal of strongly bonded oxygenated species on Pt through an intra-alloy electron transfer [48, 49]. Chemisorption of hydrogen molecules occurs more easily on oxide-free Pt surfaces [50-52]. X-ray photoelectron spectroscopy (XPS) suggests the presence of a relatively lower Pt-oxide content on a PtCo alloy compared to bare Pt [48, 49]. From the ex-situ screening and XPS analysis of different Pt systems, we have selected the PtCo system for validating this approach in a single cell PEM electrolyser. The PtCo catalyst showed the capability to reduce significantly the hydrogen concentration in the oxygen stream at the anode in the presence of a PFSA membrane with reduced thickness. This approach allows for a large increase in reaction rate while avoiding safety issues.

2. Experimental

The Pt-based hydrogen oxidation catalysts here investigated were two Pt alloys, i.e. PtRu (60:40 at.) and PtCo (75:25 at.), and Pt black. These recombination catalysts were synthesised by the sulphite complex procedure [53] to form amorphous oxides. These were successively reduced in diluted hydrogen (10 % vol. H_2 in argon at 300 °C) to form unsupported catalysts. Compared to conventional supported Pt catalysts, carbon support was avoided. At the anode of an electrolysis process, the high operating potential window causes rapid oxidation of carbon to CO_2. The catalysts were preleached in 0.1 M perchloric acid at 80 °C in order to remove both impurities and unalloyed atoms from the surface.

The Pt-based catalysts were first assessed in terms of H_2 oxidation/recombination capability in the presence of oxygen in a packed bed catalytic reactor operating at 80 °C and atmospheric

pressure. Isothermal profiles of reagents and products were acquired by using a quadrupole mass spectrometer as an analytical tool (Thermo^{Star}) equipped with a heated (150 °C) fast-response inlet capillary system. The catalyst was preliminarily treated under O_2 atmosphere, after which a mixture H_2/O_2, with a nominal hydrogen percent in the oxygen stream of 4 vol. % (simulating extreme operating conditions for the cell), was admitted into the reactor, maintaining stationary conditions until the stabilization of signals was reached. Thereafter, the catalyst was exposed to hydrogen atmosphere before to start a new cycle.

The down-selected PtCo catalyst was assessed in situ for the conversion of permeated hydrogen. A pressurised cell set-up was used in combination with a microgas cromatograph (Varian Micro GC). The scheme of the electrolysis plant in shown in Fig. S1 (supplementary data).

For the single cell characterisation, a short-side chain Solvay Aquivion® (Fig. S2, supplementary data) membrane (E98-09S) was used in combination with IrRuOx (70:30 at.) at the anode and 30% Pt/C (Ketjenblack® carbon) at the cathode of the PEM electrolyser (Fig. S3, supplementary data). Catalysts and membrane properties are described in previous papers [16,17,19]. The membrane-electrode assembly preparation was carried out according to a catalyst-coated membrane (CCM) approach by spraying the catalyst ionomer inks onto the membrane as reported in Ref. [19]. CCMs were hot-pressed at 190 °C to favour hot bonding of the catalytic layers to the membrane at a temperature higher than the glass transition temperature of the Aquivion® polymer. In the bare MEA, the catalyst - ionomer ink consisted of 25% wt. Aquivion® ionomer (D98-06AS) and 75 % wt. Pt/C catalyst at the cathode, and 15% wt. Aquivion® ionomer and 85 % wt. IrRuOx catalyst at the anode.

The PEM electrolysis cell was operated up to a current density of 3 A cm^{-2} in the presence of low Pt (0.2 mg Pt cm^{-2}) and IrRuOx (0.3 mg Ir+Ru cm^{-2}) loadings at the cathode and anode, respectively. The approach of both minimising the precious metal loadings with respect to the state-of-the art (2-3 mg cm^{-2} Ir at the anode and 0.5 mg cm^{-2} Pt at the cathode) and increasing the operating current density is one of the preferred routes to decrease the capital costs of the PEM electrolysis system [16,17,54].

In the MEA modified with the hydrogen oxidation catalyst, the specific unsupported Pt-Co alloy was coated onto the membrane and the IrRuOx layer was coated on the top to form a dual layer anode. A spraying technique was used and the Aquivion® ionomer content in both composite anode inks was kept at 15% wt. The Pt loading in the oxidation layer at the anode was 0.1 mg cm^{-2}, the other catalyst loadings were the same of the bare MEA.

Titanium diffusion layers/current collectors (Bekaert Toko Metal Fiber Co.) were used at both anode and cathode in contact with the CCM. No Pt coating was used for these diffusion layers to avoid interfering with the PtCo catalyst for the hydrogen oxidation at the anode.

An ITM POWER (UK) pressurised electrolysis single cell test fixture was used in combination with an in house (CNR-ITAE) developed test station (Fig. S1, supplementary data). The active area (geometrical electrode area) of the MEA was 8 cm^2. A power supply (TDK GEN 25-400-MD-3P400) was used to carry out polarisation experiments. An Autolab Metrohm potentiostat /galvanostat equipped with a 20 A current booster and FRA (frequency response analyser) was used to perform electrochemical impedance spectroscopy (EIS). Polarization curves were performed in the galvanostatic mode by recording the cell voltage vs. the imposed current density. A stepwise increase of current was used. Electrochemical impedance analysis was performed in the potentiostatic mode at 1.5 V and 1.8 V. The frequency was varied from 100 kHz to 100 mHz in the single sine mode with a sinusoidal excitation signal of 10 mV pk-pk. In all experiments, milli-Q Integral, Millipore deionized water was heated at 55 °C before being supplied to the cell anode with a flow rate of 1 $mL \cdot min^{-1}$ cm^{-2}. The inlet water temperature was assumed as the cell temperature.

Physicochemical properties of the materials were examined by scanning electron microscopy – energy dispersive X-ray analysis (SEM-EDX) using a FEI FEG–XL30 instrument, transmission electron microscopy (TEM) was carried out with a FEI CM12 microscope and X-ray diffraction (XRD) was made by using a Panalytical X-Pert diffractometer equipped with a CuKa as radiation source. X-ray photoelectron spectroscopy was carried out with a PHI 5800-01 spectrometer. Spectra were obtained using a monochromatic Al Ka X-ray source and acquired with a pass energy of 187.85 eV for survey and 11.75 eV for high resolution spectra, respectively. BET (Brunauer, Emmett and Teller) surface area of the catalysts was measured with Thermo Fisher Scientific sorptomatic instrument.

3. Results and discussion

3.1 Structural and chemical characterisation of the Pt-based recombination catalysts

With regard to the hydrogen oxidation catalysts investigated in this study, PtRu was selected to obtain a bifunctional effect for H_2 oxidation at the Pt sites and water oxidation on the surface of RuOx species which are formed under anodic conditions [52]. PtCo was instead chosen because cobalt in the alloy can transfer electrons to platinum atoms thus keeping Pt in a reduced state

[48,49]. For the PtRu catalyst, in order to promote water oxidation in combination with hydrogen oxidation/ recombination, the selected Ru concentration was larger than that of Co in the alloy.

The atomic ratio for both bimetallic samples was studied by energy dispersive X-ray analysis (EDAX) after a pre-leaching in perchloric acid (Fig. S4, supplementary data). The final atomic ratio was 75:25 for the PtCo and 60:40 for the Pt:Ru. EDAX spectra showed larger oxygen content in PtRu compared to the other catalysts (Fig. S4).

Structural and morphological analyses (Figs. 1-2) showed a good dispersion and a face-centered cubic phase for both Pt alloys [53, 55-58]. The peak shift towards higher Bragg angles compared to Pt black (Fig. 1b) indicates in both cases the occurrence of an alloy. The observed shift is in accordance with the atomic contents in the bimetallic systems [53, 55-58]. From the broadening of the diffraction peaks (Figs. 1a-b), a crystallite size of 6.4, 2.7 nm and 6.9 nm was determined for Pt black, PtRu and PtCo, respectively, by using the Debye-Scherrer law.

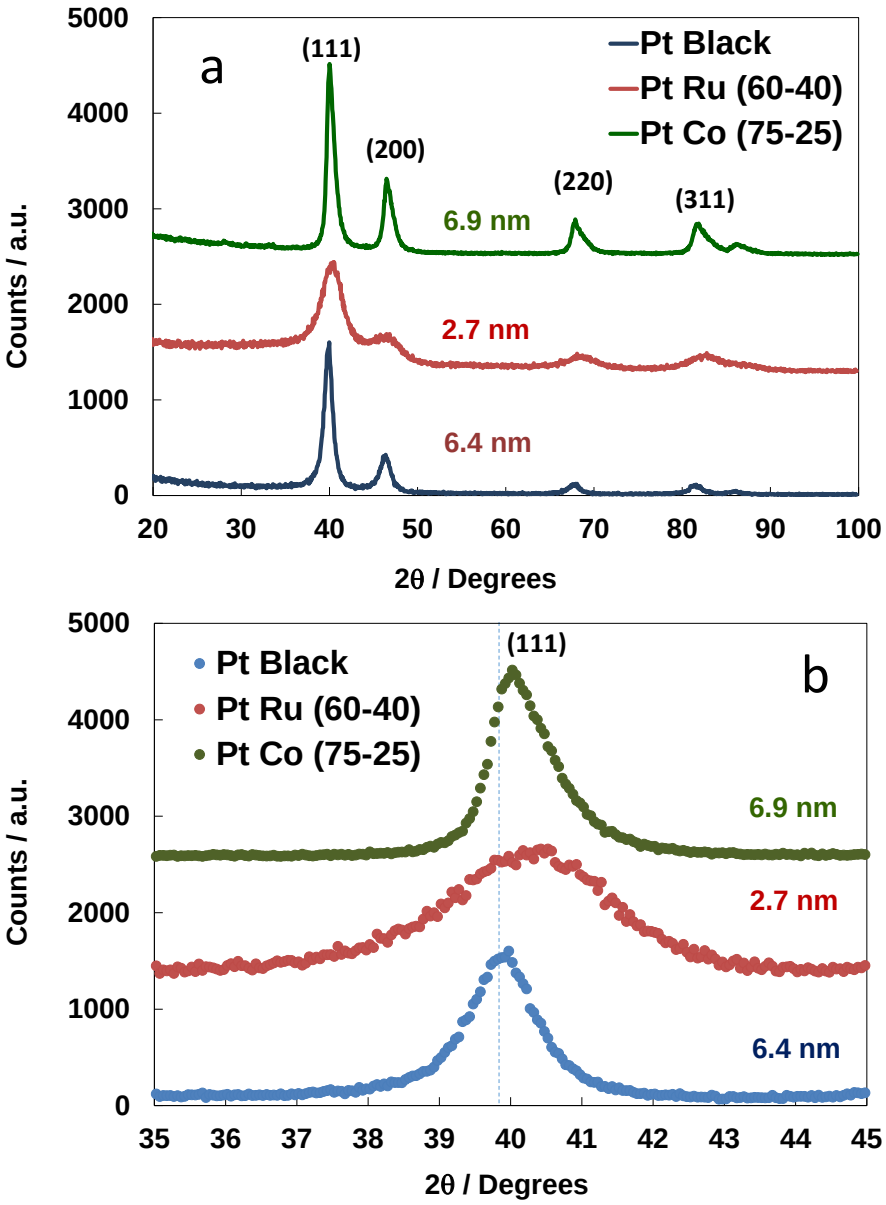

Fig. 1 X-ray diffraction patterns of the recombination/hydrogen electro-oxidation catalysts; a) full range; b) magnification of the Pt (111) reflection region.

SEM analysis (Fig. 2) showed a sponge-like structure characterised by fine particles for all these unsupported catalysts. TEM analysis showed the presence of properly dispersed catalyst agglomerates which were composed of finer particles in the case of the PtRu unsupported catalyst compared to PtCo (Fig. 2). The Pt particle size in Pt black was in between that of PtRu and PtCo. Due to the relevant agglomeration, which is very common for the unsupported catalysts, it is not easy to estimate precisely the particle size distribution. However, it is clear that the presence of Ru mitigates the growth of the Pt particles during the thermal reduction in hydrogen determining a finer structure (Fig. 2) with a crystallite size from XRD much lower than that of Pt black and PtCo

(Fig. 1). This is also evident from TEM analysis at higher magnification (Fig. S5 supplementary data).

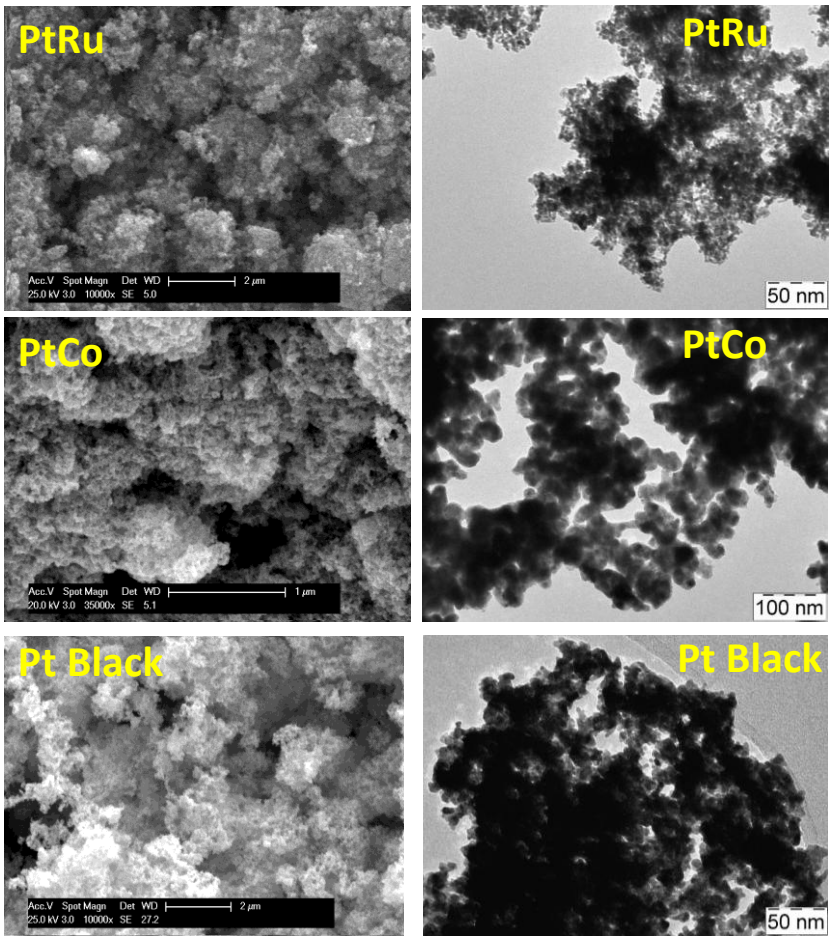

Fig. 2 Scanning (left) and transmission (right) electron micrographs of the recombination / hydrogen electro-oxidation catalysts

3.2 Assessment of the Pt-based catalysts for the hydrogen oxidation/ recombination in the gas-phase

The PtCo catalyst showed excellent recombination properties and it was selected for further assessment in the electrolysis cell. In fact, in the packed bed catalytic reactor, when hydrogen was fed at 4% in an oxygen stream (flammability limit), 99.5% of the total H_2 content was immediately converted to water thus avoiding safety issues. Thus, since 99.5% of H_2 was converted at the PtCo catalyst, this was corresponding in our experiments to 0.02 % residual H_2 (4%·99.5%). Moreover, the dynamic H_2 conversion response and the conversion rate under a steady-state regime remained optimal with the number of cycles (Fig. 3).

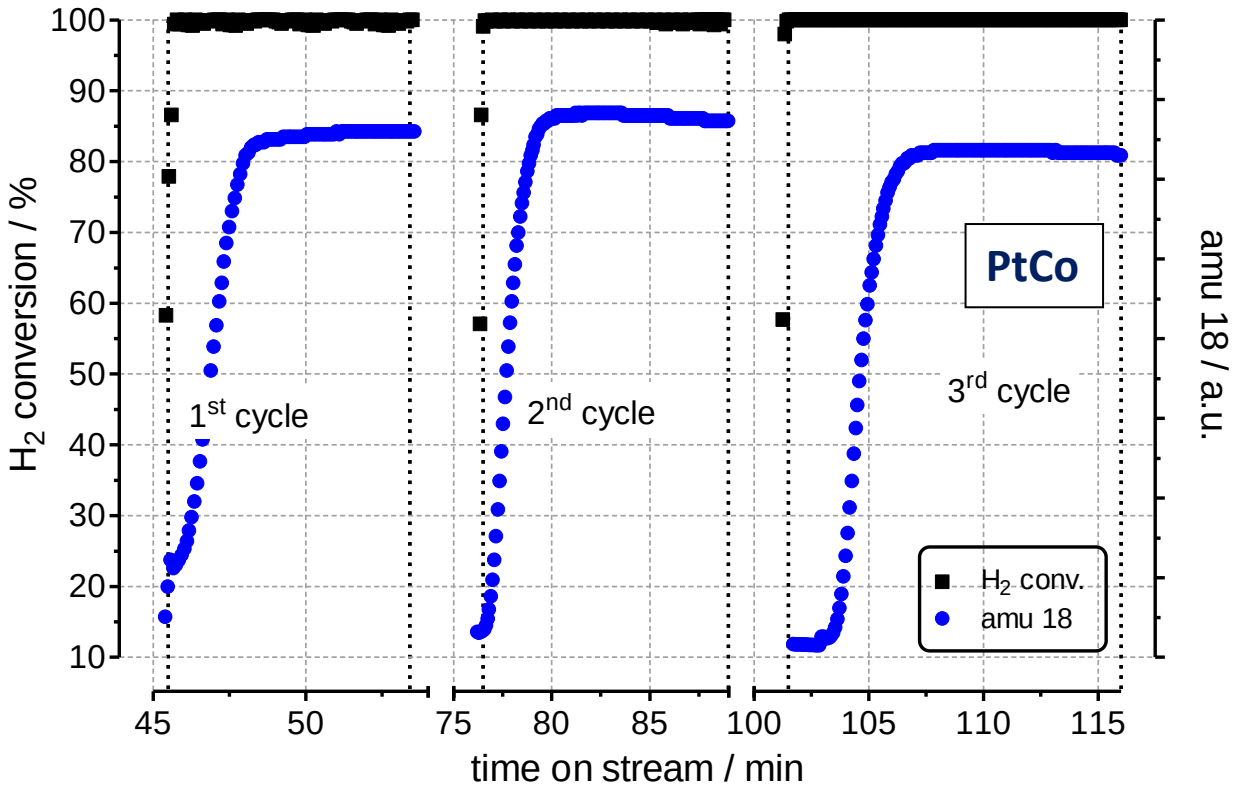

Fig. 3 Hydrogen conversion and water formation (H_2O = 18 amu-atomic mass unit) as a function of time at PtCo in a packed-bed catalytic reactor upon 4% vol. H_2 feed in a pure oxygen stream (three cycles). In each cycle, the catalyst was exposed to pure oxygen before feeding the 4% vol. H_2 – 96 % vol. O_2 mixture.

On the contrary, the H_2 conversion was relatively poor for the PtRu alloy compared to the PtCo system and the recombination performance significantly decreased with the number of cycles (Fig. 4). These results are essentially ascribed to a chemisorption of oxygen on the Ru sites [58]. Water is formed during this process. According to the well-known water displacement effect on the surface of the PtRu [52], this catalyst favours the surface uptake of oxygen species instead of adsorbed hydrogen intermediates. This process is well-known in aqueous solutions where formation of Ru-OH and Pt-OH species instead of Pt-H occurs on PtRu [59]. This is favourable for the electro-oxidation of alcohols and CO in fuel cells but it reduces the reaction kinetics for H_2 oxidation [59]. As matter of evidence, cyclic voltammetry analysis of PtRu catalysts in the "so-called" hydrogen region does not provide a clear evidence of the Pt-H peaks because of the strong overlapping with the adsorbed OH species [60]. This phenomenon does not occur in the cyclic

voltammetry analysis of PtCo where the under-potential hydrogen adsorption peaks are well observed [25, 49, 51, 53].

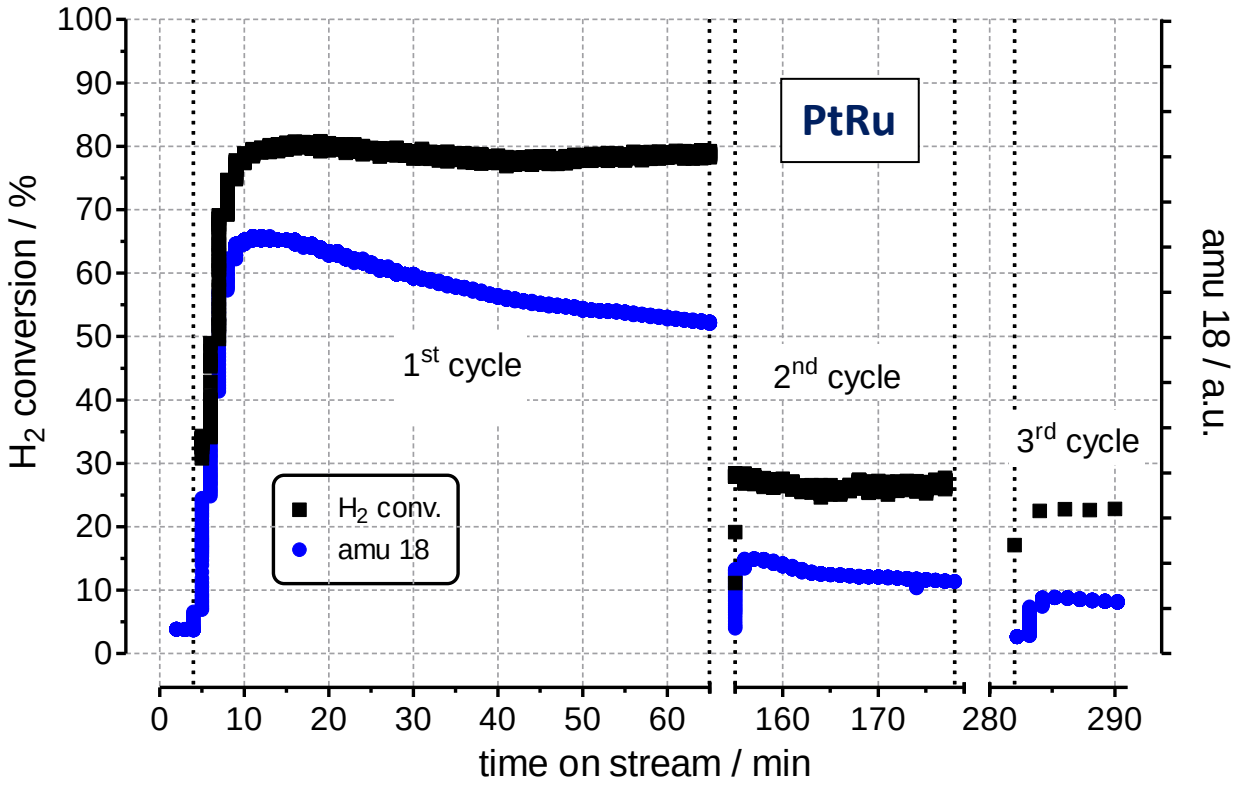

Fig. 4 Hydrogen conversion and water formation (H_2O = 18 amu-atomic mass unit) as a function of time at PtRu in a packed-bed catalytic reactor upon 4% vol. H_2 feed in a pure oxygen stream (three cycles). In each cycle, the catalyst was exposed to pure oxygen before feeding the 4 % vol. H_2 – 96 % vol. O_2 mixture.

The recombination performance of the Pt black catalyst was similar to that of the PtCo (Fig. 5a) even if the dynamic response appeared slower (Fig. 5b).

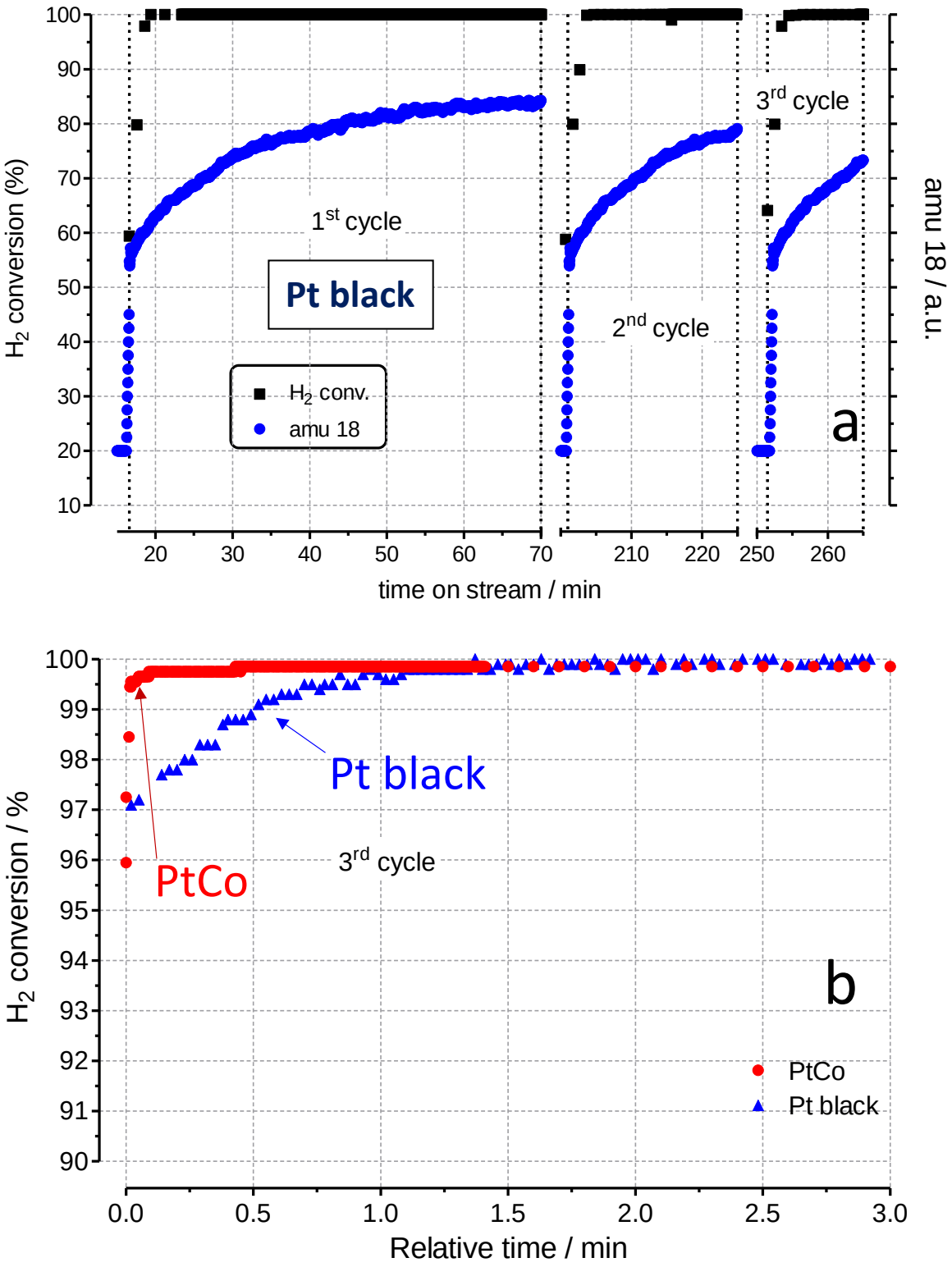

Fig. 5 a) Hydrogen conversion and water formation (H_2O = 18 amu-atomic mass unit) as a function of time at Pt black in a packed-bed catalytic reactor upon 4% vol. H_2 feed in a pure oxygen stream. In each cycle, the catalyst was exposed to pure oxygen before feeding the 4 % vol. H_2 – 96 % vol. O_2 mixture. b) Comparison of H_2 conversion response versus time for PtCo and Pt black catalytic systems after three cycles.

3.3 Surface characterisation of the Pt-based catalysts

The three catalysts were also characterised in terms of surface properties by X-ray photoelectron spectroscopy. By comparing the Pt 4f photoelectron peaks of the three catalysts (Fig. 6), it is evident that the sample characterised by a larger fraction of metallic platinum on the surface is the PtCo catalyst, in accordance with the previous literature reports [48]. The Pt $4f_{7/2}$ peak occurs at 71.30 eV for PtCo, 71.40 eV for Pt black and 72.1 eV for PtRu. The broadening and shift to higher binding energy of the Pt $4f_{7/2}$ peak together with the peculiar shape of the overall Pt4f profile for the PtRu catalyst (the intensity ratio between $Pt4f_{7/2}$ and $Pt4f_{5/2}$ should be 4:3 in a pure Pt metal) reveal the presence of a significant fraction of oxidised species in this sample. This in part occurs also in the Pt black catalyst, even if in a much lesser extent, compared to PtRu. Such evidences were confirmed by peak deconvolution analysis (Fig. S6, supplementary data). The concentration of oxidised species (Pt^{2+} and Pt^{4+}) was 69 % in the PtRu catalyst, 37% in the Pt black and 25% in the PtCo bimetallic alloy (Table S1, supplementary data).

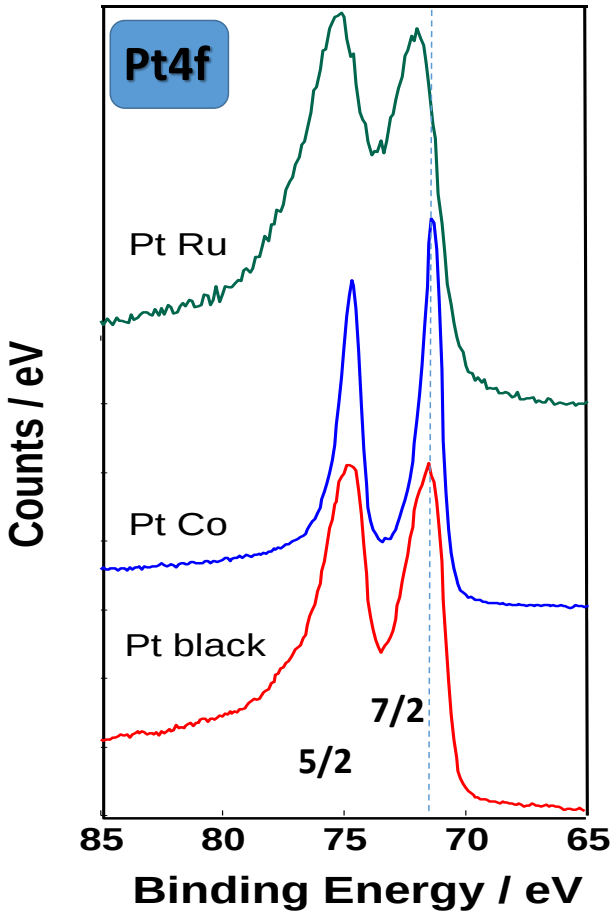

Fig. 6 High resolution X-ray photoelectron spectra of the Pt4f region of the recombination/hydrogen electro-oxidation catalysts

Despite the fact that the PtCo catalyst was pre-leached in $HClO_4$ as final preparation step, the XP-survey spectrum shows the presence of both Pt and Co on the surface with modest occurrence of carbon and oxygen from adsorbed adventitious species (Fig. S7). O1s and C1s signals essentially derive from adsorbed organic species as confirmed by their significant reduction after a very mild sputtering of 10 min with Ar^+ ions (Fig. S8). The presence of Co in the outermost layers indicates a strong interaction with Pt causing acharge transfer which allows keeping Pt sites mostly in a reduced state.

According to these evidences and the gas-phase catalytic results, PtRu and Pt black were excluded from a further assessment in the electrochemical cell in favour of the PtCo system.

3.4 Single cell electrochemical assessment of a Pt-Co alloy for the hydrogen oxidation at the anode compartment of a PEM electrolysis cell

A comparison of the cross-sections of the membrane-electrode assemblies for the MEAs with and without the Pt-Co oxidation catalyst at the anode is shown in Figure 7. The anode catalyst appears much thinner and less regular than the cathode catalyst as consequence of the much larger density and significantly lower surface area of IrRuOx (150 m^2/g) compared to Ketjenblack® carbon (about 900 m^2/g) in 30% Pt/C (Fig. 7a). In the case of the modified MEA, a 0.1 mg PtCo cm^{-2} was integrated in the anode in between the membrane and the IrRuOx catalyst (Fig. 7b) by using a spray coating technique. An analysis at higher magnification of the interface between the membrane and the dual-layer anode allows identifying the PtCo oxidation layer (Fig. 7c). This is very thin (about 4 microns) due to the high mass density of this unsupported catalyst. A good adhesion of the dual layer anode to the membrane is also observed (Fig. 7b-c).

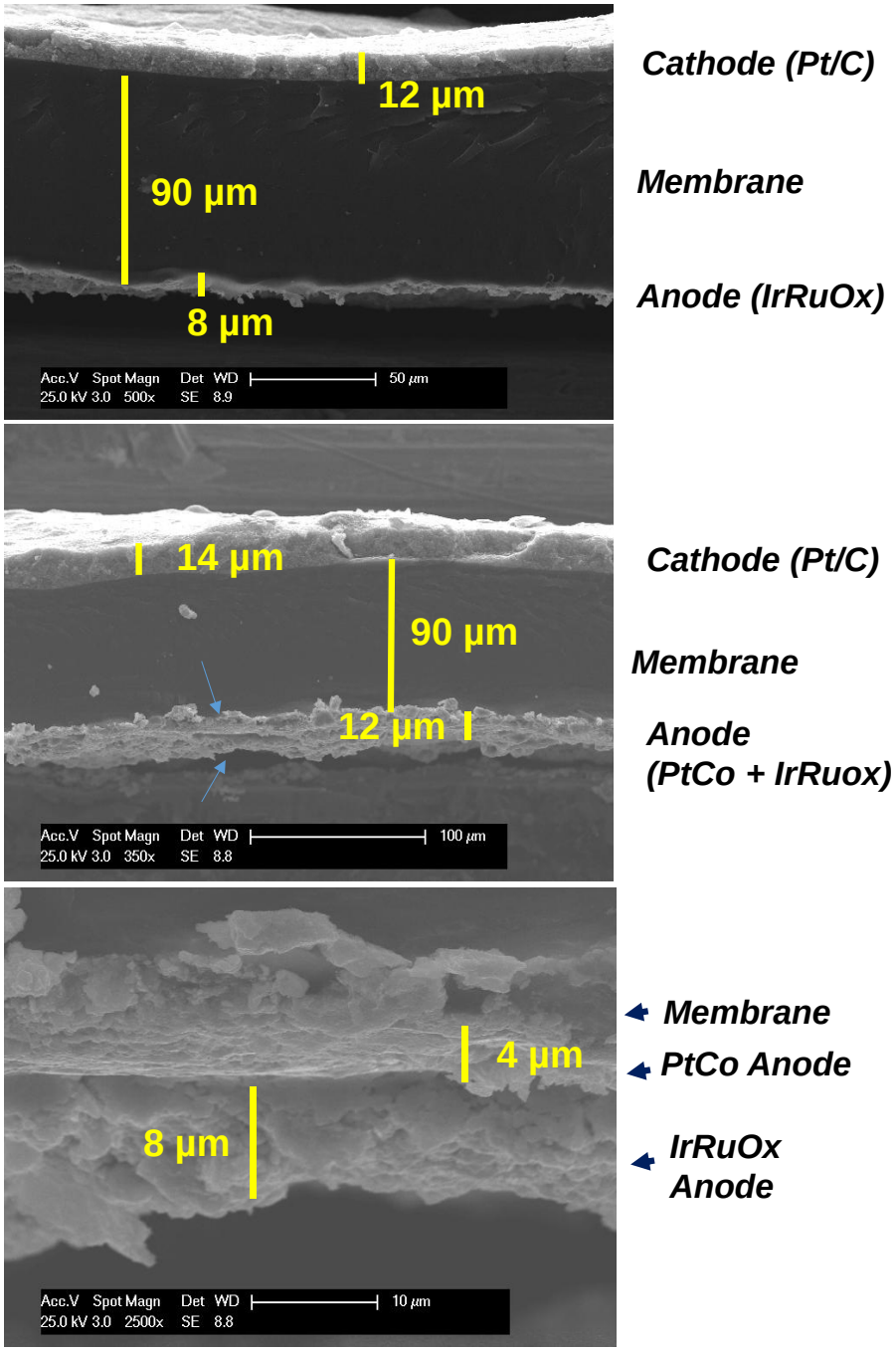

Fig. 7 Scanning electron micrographs of the MEAs (a) without and (b) with the PtCo hydrogen electro-oxidation catalysts

Single cell polarisation measurements at almost ambient pressure (1 bar differential pressure) of bare and PtCo-modified MEAs showed a slightly better performance of the cell containing the Pt-Co hydrogen oxidation catalyst showing about 100 mV lower cell voltage in almost all the overall range of current density (Fig. 8a). In particular, the enhanced performance was more evident at lower current densities in the activation-controlled region. This could be probably due to both the enhanced oxygen evolution (although Pt is less

performing than IrOx for oxygen evolution [61-64], the additional Pt catalyst layer produces some effect being about 25% of the overall anode catalyst) and the oxidation of the permeated hydrogen. The latter process is very fast on Pt at high potentials [25]. Thus, the permeated hydrogen was very likely oxidised to H^+ ions in the acidic environment at the PtCo catalyst. The formed protons back diffused to the cathode where they were reduced again to molecular hydrogen. This parasitic process does not contribute to the final amount of produced hydrogen in the outlet stream of the electrolyser; however, it affects the polarisation curve causing a depolarisation effect by means of such internal parasitic current.

Interestingly, when a differential pressure of 20 bars is applied between the cathode and anode (pressurised hydrogen, 20 bar gauge pressure; unpressurised oxygen, ambient pressure), the difference between the polarisation characteristics of the two MEAs is less relevant (Fig. 8b). The cell voltage of the PtCo - modified MEA is 30 mV lower than the bare MEA up to about 2 A cm^{-2}. The performance of these MEAs is similar at very high current density (Fig. 8b). Whereas the catalytic effect of PtCo is evident only in the low current density region.

There are some relevant aspects in the polarisation curves at 20 bar (Fig. 8b) that require a specific discussion. At low current density, an upward shift of the cell voltage for the curves at 20 bar (Fig. 8b) compared to the experiment at ambient pressure (Fig. 8a) is observed. This because of a positive shift with the pressure of the reversible potential for water splitting according to the Nernst law [21]. In addition, a flattening effect for the polarisation curves at 20 bar is observed at high current density (Fig. 8b). There are essentially two effects causing such peculiar behaviour. First, the water temperature is controlled at the cell inlet by a thermostat and this is assumed as the nominal cell temperature. During the pseudo-steady state polarisation measurements at high current density (data are collected when the cell performance stabilizes), there is an internal increase of the local temperature that is caused by the exothermic electrolysis reaction at potentials well above the thermoneutral potential [16]. In effect, an increase of cell temperature (some degrees Celsius) is recorded for the outlet water during operation at high current density. This causes a decrease of the cell potential because both the membrane conductivity and the reaction kinetics are significantly enhanced by the increase of internal temperature [65]. The low water flow rate used in our experiments does not allow to efficiently extracting the produced heat. A second effect is due to the formation of finer hydrogen bubbles at high pressure reducing the mass transport

constraints at high current density [66]. Thus, both the increase of the local temperature (increase of membrane conductivity and reaction kinetics) and the decrease of mass transport constraints, under high operating pressure, produce a decrease of cell voltage at high current density that is counteracted by the increase of ohmic drop with the current. The balance between these two opposite effects results in a flattening of the cell potential vs. current density profile in the high current density region compared to low operating currents. These aspects are also investigated using electrochemical impedance spectroscopy (see below).

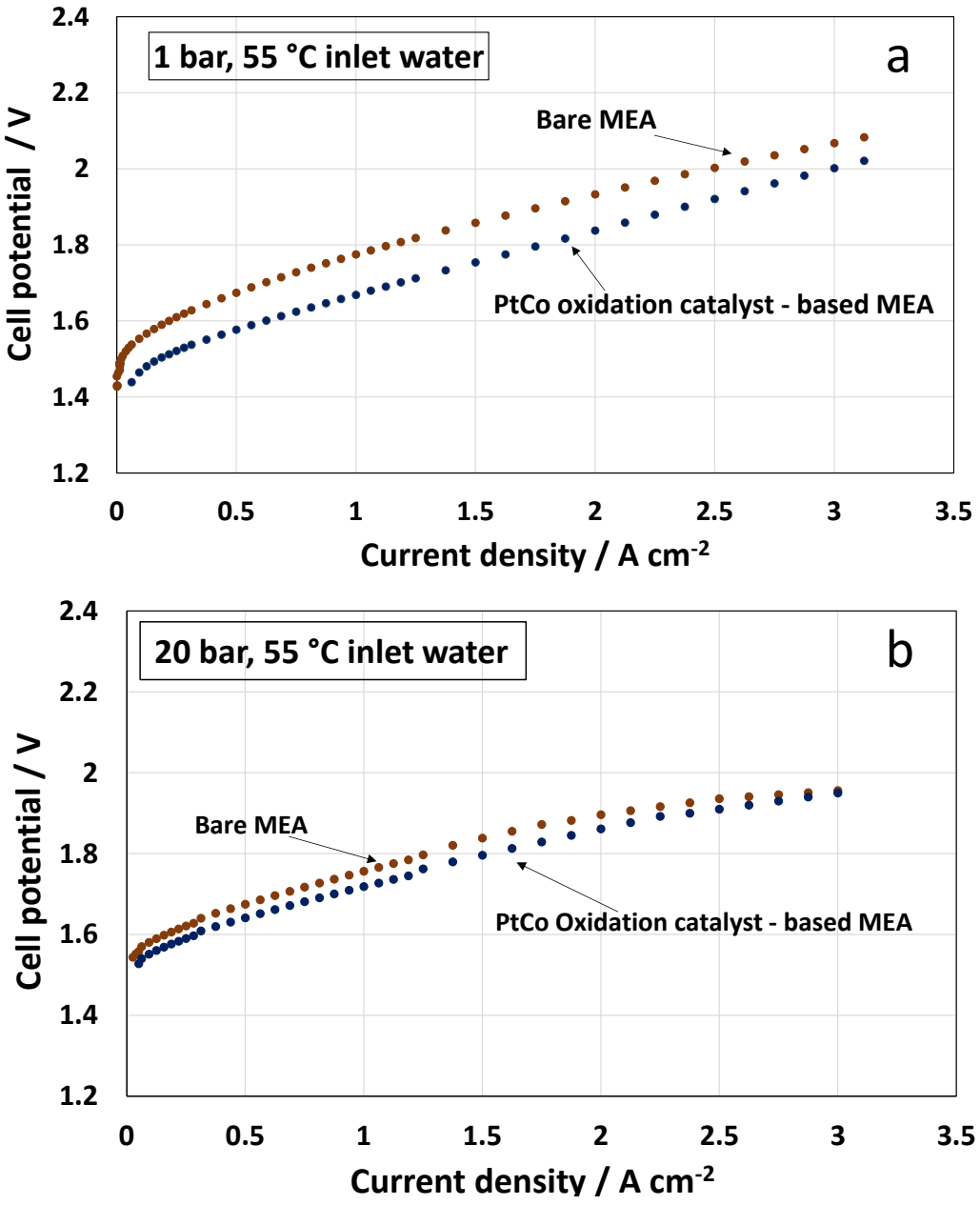

Fig. 8 Electrolysis polarization curves for the bare MEA and the MEA containing the PtCo oxidation catalyst at (a) 1 bar and (b) 20 bar differential pressure, at a constant water inlet temperature of 55 °C.

Considering that the thermoneutral potential is about 1.5 V under such conditions, a voltage efficiency of 77% is achieved at 3 A cm^{-2} and 20 bar. It is interesting to note that at high pressure the polarisation curves for the bare and PtCo-based MEAs overlap at high current densities (Fig. 8b). This despite the fact that the permeated hydrogen is oxidised at the PtCo anode contributing in principle to the overall electrochemical reaction rate. However, at high overpotentials, also O_2 evolution is greatly enhanced. Under such conditions, the use of the additional PtCo catalytic layer does not produce a positive effect on the electrochemical reaction rate since the IrRuOx layer where oxygen evolution occurs is not in contact with the membrane. Usually, an intimate contact between IrRuOx and membrane favours the oxygen evolution process.

The measurements of the hydrogen gas concentration in the oxygen stream (anode) at ambient pressure (Fig. 9a), clearly show a relevant decrease of the hydrogen content in the overall range of current densities in the presence of a PtCo catalyst. The effect appears more relevant at the low operating current densities where a mitigation action is more important. At ambient pressure, there is almost 50% reduction of the H_2 concentration in oxygen in a wide range of current densities.

The reduction of the H_2 concentration in the oxygen stream is also relevant at 20 bar (Fig. 9b) even if it is less significant compared to what observed at ambient pressure. Probably, due to the thin unsupported PtCo catalyst layer over the membrane, the occurrence of preferential pathways for hydrogen permeation may occur under high differential pressure operation. However, the reduction of the hydrogen content in the anode stream appears similar at both operating pressures at least in terms of absolute values (Figs. 9a-b).

It is important to consider that, the excellent capability of the PtCo to act as recombination catalyst in the gas catalytic process was in part favoured by the presence of a thick and dense catalytic layer in the packed-bed reactor. Unfortunately, the need to reduce the Pt content in the electrochemical cell does not allow using a thick PtCo layer in the electrolysis MEA. The trade-off between the enhancement of the hydrogen production rate in the electrolysis system using a thin membrane and the increase of catalyst cost contribution by effect of the additional PtCo oxidation catalyst layer needs to be investigated more in-

depth. However, for the present 90-µm membrane, the addition of just 0.1 mg cm^{-2} of PtCo hydrogen oxidation catalyst produces a decrease of the concentration of hydrogen in the oxygen stream well below the flammability limit of 4% also at a current density of 0.15 A cm^{-2}. Considering a nominal operating current density of 3 A cm^{-2} for this system [16, 17], the PtCo hydrogen oxidation catalyst allows to extend the minimum partial load operation down to 5% whereas commercial systems usually do not allow partial load operation below 20% and 0.3 A cm^{-2} [8, 9, 14, 67].

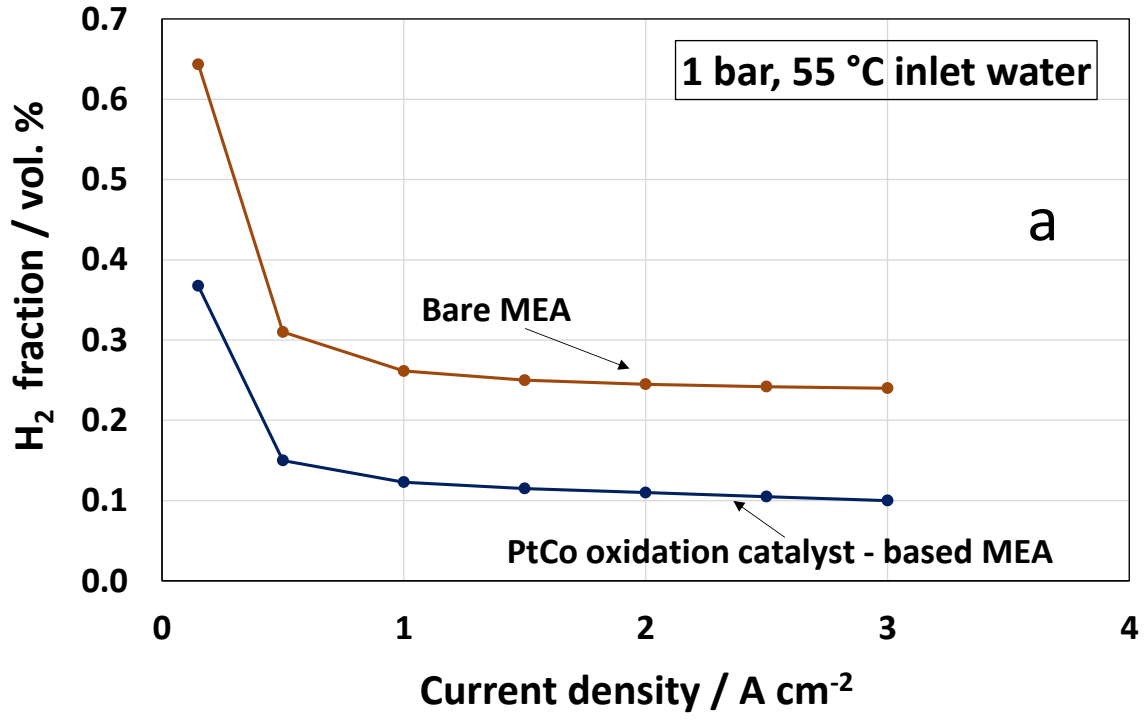

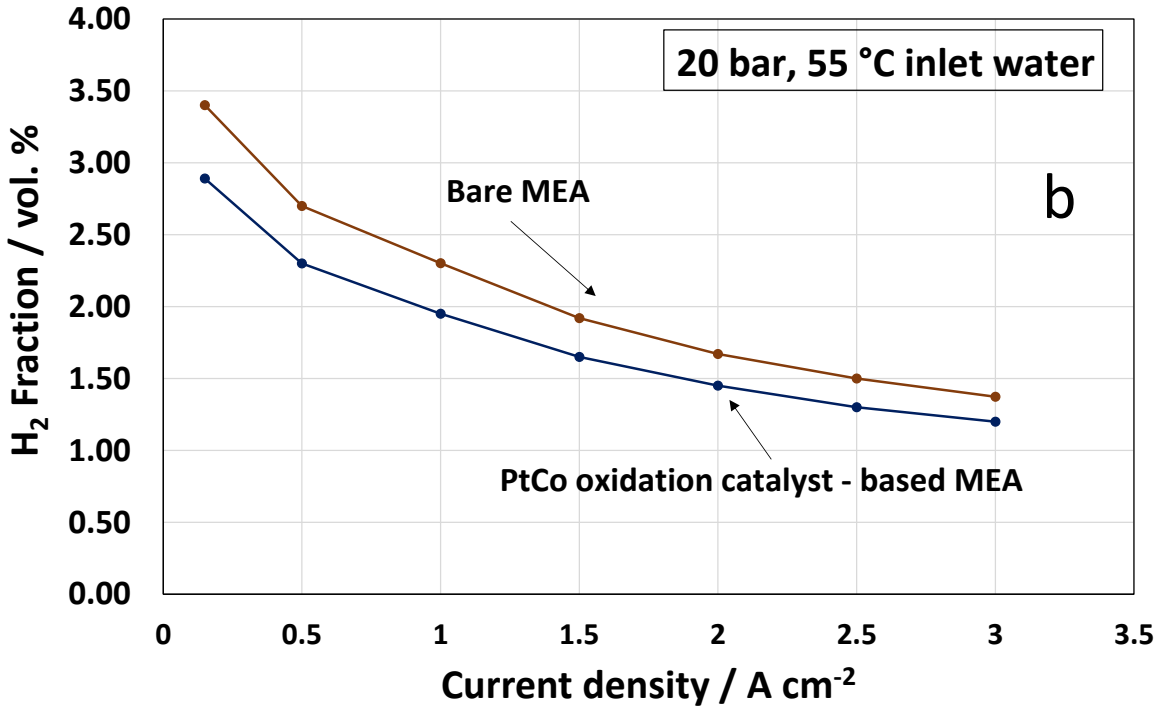

Fig. 9 Hydrogen fraction in the outlet anode stream at various current densities for the bare MEA and the MEA containing the PtCo oxidation catalyst at (a) 1 bar and (b) 20 bar differential pressure, at a constant water inlet temperature of 55 °C.

The equivalent current density for the hydrogen permeation rate into the anodic outlet stream was estimated, at different operating electrolysis current densities, from the measured H_2 concentration in the anode stream and the oxygen production rate according to the following formulas:

$$\mathrm{C}_{H_2} = \frac{\mathrm{mol}_{H_2}^{permeated}}{\mathrm{mol}_{H_2}^{permeated} + \mathrm{mol}_{O_2}^{evolved}} \; ; \qquad (1)$$

$$\mathrm{I}_{H_2}^{permeated} = 2 \cdot F \cdot \mathrm{mol}_{H_2}^{permeated}; \qquad \text{Faraday's law} \qquad (2)$$

Where C_{H_2} is the experimentally determined concentration of hydrogen in the outlet anode stream; $\mathrm{mol}_{O_2}^{evolved}$ are the number of evolved oxygen moles per unit of time; $\mathrm{mol}_{H_2}^{permeated}$ are the calculated number of hydrogen moles per unit of time released into the anodic outlet stream; $\mathrm{I}_{H_2}^{permeated}$ is the equivalent current density for the hydrogen permeation rate, 2 is the number of electrons exchanged during the oxidation of one hydrogen molecule and F is the Faraday's constant.

This calculation neglects the oxygen cross-over to the cathode [68] that in our high differential pressure experiments (hydrogen pressurised at 20 bar, non pressurised oxygen) is relatively low (<1%) compared to the overall produced oxygen. This is confirmed by the comparison of the amount of oxygen evolved at the anode and the nominal oxygen production calculated from the Faraday's law at specific current densities.

The equivalent current density for the hydrogen permeation into the outlet anode stream, at various electrolysis current densities, for the bare MEA and the MEA containing the PtCo oxidation catalyst, at 1 bar and 20 bar differential pressures, is shown in Fig. 10a-b. It is observed that the hydrogen permeation rate increases linearly, as also observed in the literature [22], especially at high operating current densities (Fig. 10 a-b). This permeation process is particularly related to the oversaturation of hydrogen in the cathode catalytic layer [22]. The oversaturation increases proportionally with the electrolysis current density. At almost ambient pressure and very low current densities, the diffusion process may be

essentially driven by the concentration gradient [69]. The slope of the curve is lower under such conditions (Fig. 10a).

When the differential pressure was increased at 20 bar (Fig. 10b), the permeation rate was significantly higher than at ambient pressure. In this case, the permeation rate also increased linearly with the current density but according to two different slopes. The slope was higher at low current density (Fig. 10b). According to the high pressure conditions, a supersaturation of the cathode layer with H_2 is also occurring in this range and hydrogen permeation at low current densities is facilitated by a lower oxygen production at the anode side. Of course, this phenomenon is critical for the system safety [67]. The observed hydrogen permeation rate into the anode outlet decreases in the presence of the PtCo catalyst, at both pressures (Fig. 10a-b), as this catalyst converts a fraction of the hydrogen permeated through the membrane into protons.

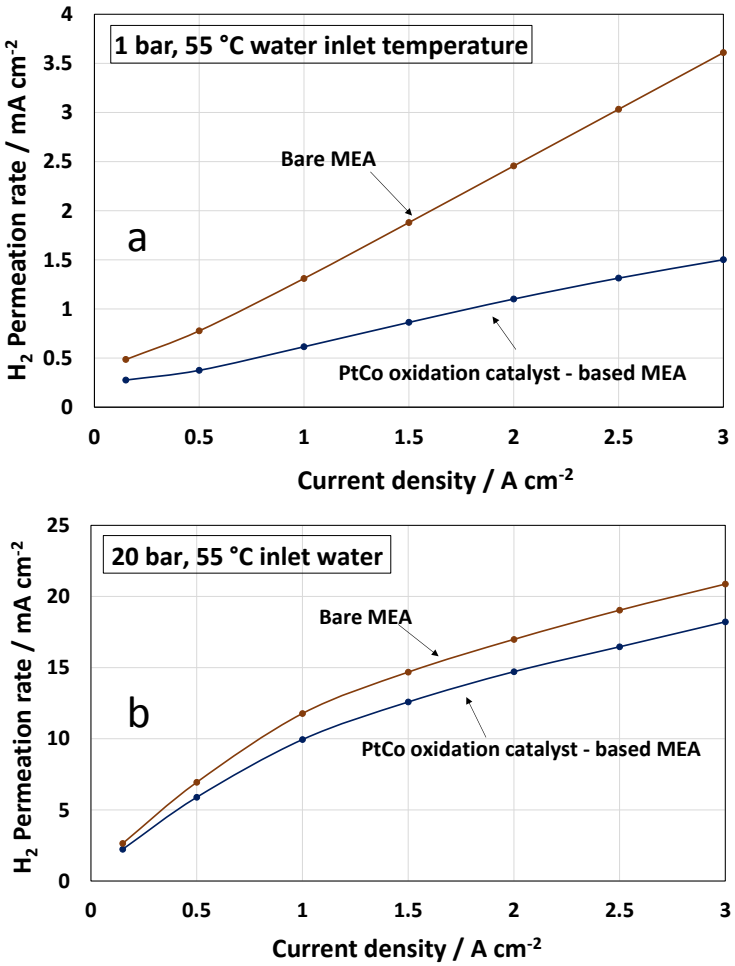

Fig. 10 Equivalent current density for the hydrogen fraction in the outlet anode stream at various electrolysis current densities for the bare MEA and the MEA containing the PtCo

oxidation catalyst at (a) 1 bar and (b) 20 bar differential pressure, at a constant water inlet temperature of 55 °C.

Faradaic efficiency was estimated from the hydrogen flow rate after a cryogenic drying (Fig. S9). At 20 bar, the faradaic efficiency was about 99% in a wide range of current densities from 0.5 to 3 A cm^{-2} for both MEAs. This high faradaic efficiency achieved in the presence of a relatively thin membrane (90 µm) clearly shows that the problem of hydrogen permeation into the anode is not affecting significantly the electrolysis efficiency but mainly the system safety especially under low current density operation.

The polarisation curves, recorded at different differential pressures, are compared in Fig. 11a. As discussed above, an increase of the cell voltage with the increase of pressure is observed at low current densities. Instead, at large current densities, the internal increase of temperature caused by a poor heat exchange, which appears more relevant under pressure, and the decrease of the size of gas bubbles with pressure play an important role. Practically, the system efficiency at high current density is improved by the increase of temperature and pressure.

Also in the presence of PtCo, the hydrogen concentration increases significantly in the low current density range (Fig. 11b). However, the safety limit becomes critical at 20 bar for a current density lower than 0.15 A cm^{-2} (Fig. 11b). One can see that a further increase of the operating pressure is possible but the safety limit for the minimum operating current density will shift towards higher currents. In other words, electrolysis systems operating at very high pressure have a smaller partial load range. The rate of hydrogen permeation with the current density increases with the pressure (Fig.10). However, the hydrogen permeation in the outlet anode stream remains relatively low compared to the amount of hydrogen produced at the cathode for the present combination of PtCo oxidation catalyst and Aquivion® membrane (90 µm).

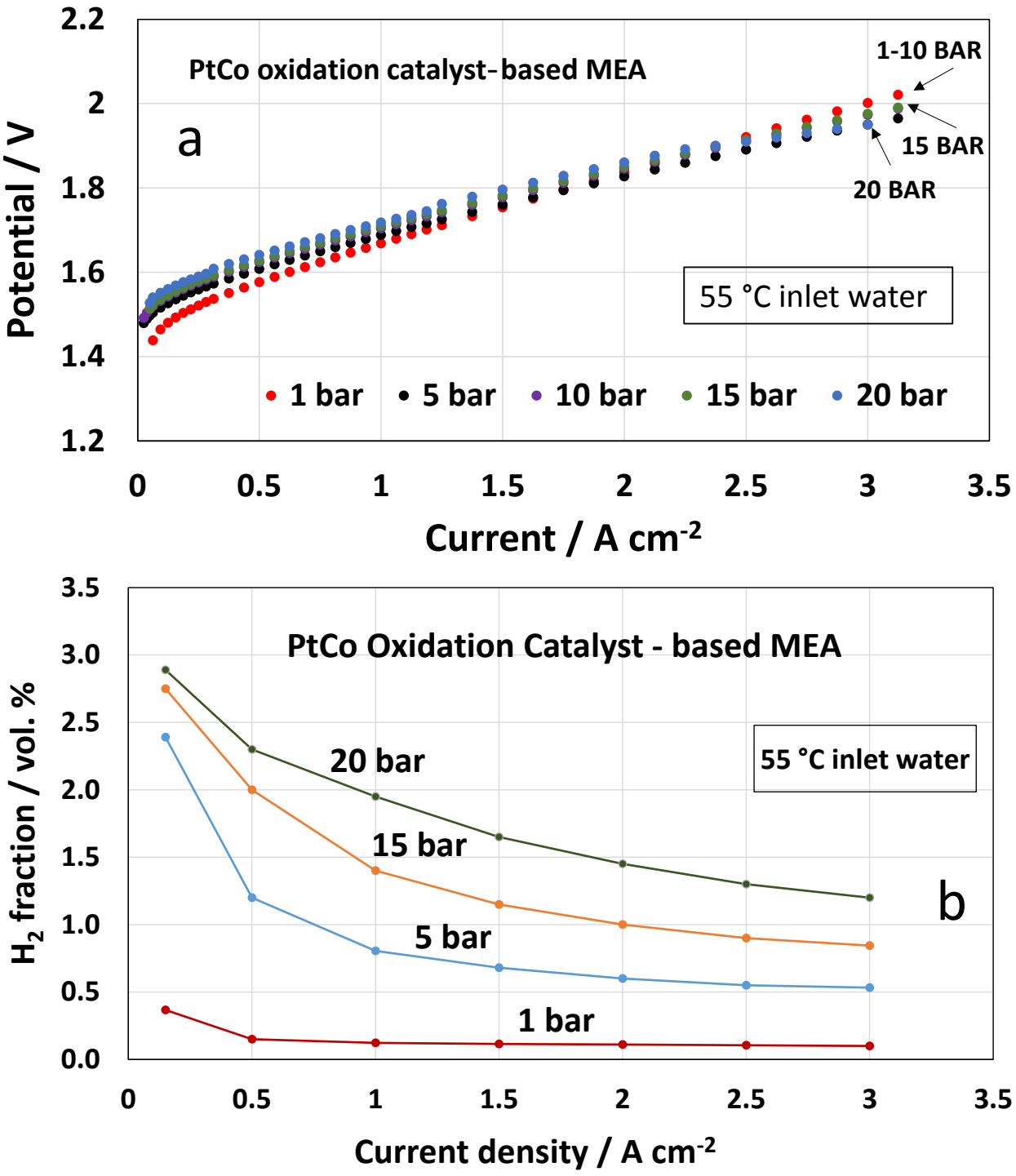

Fig. 11 Polarisation curves (a) and hydrogen fraction in the outlet anode stream (b), at different pressures, for the MEA containing the PtCo oxidation catalyst, at a constant water inlet temperature of 55 °C.

The effect of the differential pressure was also investigated, under constant voltage efficiency conditions, by electrochemical impedance spectroscopy. Nyquist plots for the MEA containing the PtCo oxidation catalyst, obtained at 1.5 V and 1.8 V, at different pressures, are reported in Figs. 12a-b. This to get insights about the limiting steps affecting the electrolyser operation in the activation-controlled region and at high current densities. At 1.5 V voltage (Fig. 12a), a single semicircle is evident in the investigated frequency range. This is essentially related to the charge transfer process associated to the oxygen evolution reaction (rate determining step under these conditions) [19,70]. As discussed above, the reversible Nernst potential shifts positively with the increase of pressure [21]. Thus, the effective applied overvoltage decreases with the increase of the operating pressure. For purely kinetic processes, the reaction rate (current density) and applied overpotential are directly related according to the Volmer-Butler equation. Thus, the increase of charge transfer resistance with the increase of pressure in this region (Fig. 12a) is essentially due to this effect.

Fig. 12b shows instead at 1.8 V a decrease of the overall differential resistance (low frequency intercept on the real axis) with pressure. Two semicircles are observed in these spectra. The high frequency semicircle is still related to the charge transfer process associated to the oxygen evolution reaction whereas the low frequency semicircle is very likely related to mass transport limitations [19,20]. At the same pressure, the charge transfer process associated to the oxygen evolution is significantly lower at 1.8 V than at 1.5 V due to the effect of the different overpotential according to the Volmer-Butler equation (Fig. 12). However, the decrease of charge transfer resistance with pressure in the high current density region (1.8 V) is possibly related to a depolarisation effect caused by the hydrogen cross-over to the anode. The decrease of the mass transfer resistance with pressure at low frequency is instead likely related to the formation of finer gas bubbles. Interestingly, at 1.8 V (Fig. 12b), there is a decrease of the series resistance (high frequency intercept on the real axis of the Nyquist plot) passing from almost ambient pressure to 20 bar differential pressure probably caused by an improved MEA compression.

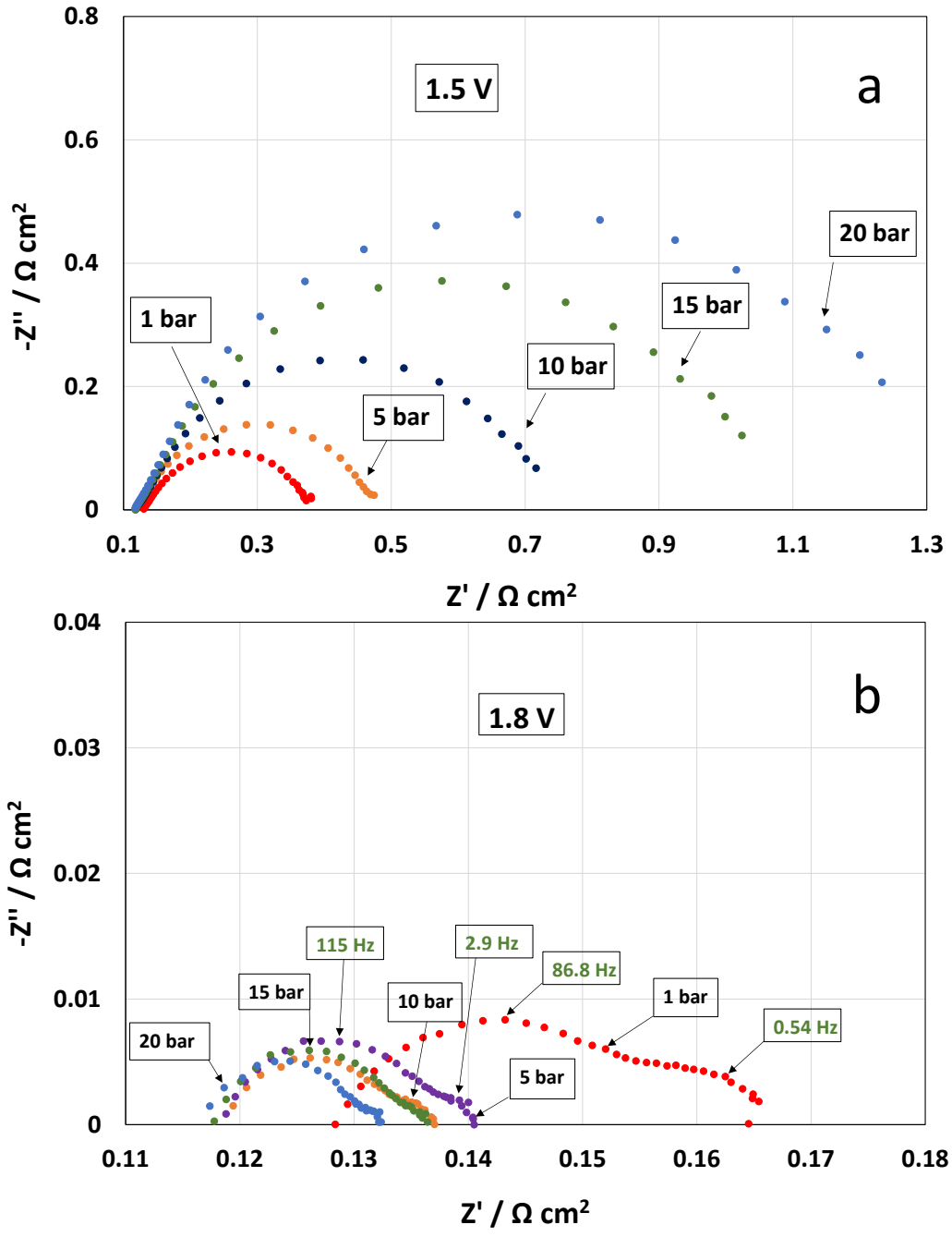

Fig. 12 Electrochemical impedance spectra, at 1.5 V (a) and 1.8 V (b), at different pressures, for the MEA containing the PtCo oxidation catalyst, at a constant water inlet temperature of 55 °C.

The present approach can allow for the use of thinner membranes in electrolysis. A comparison of the H_2 concentration in the outlet anode stream for the present system with the literature results for conventional MEAs, based on much thicker membranes (170 µm, 230 µ) is shown in Fig. 13a-b. This comparison indicates a positive role of the PtCo catalyst

especially in the low range of current density. For thick membrane based MEAs, there are not many literature data available for the hydrogen concentration in the anode stream at current densities higher than 2-3 A cm^{-2}. The reason is essentially due to the fact that the voltage efficiency for a thick membrane-based MEA is relatively low at high current density. This is due to the large ohmic drop. Thus, there is no interest in analysing the cell behaviour under conditions which are not of practical relevance. From the trend observed in Fig. 13, it may be possible that at very high current density, the concentration of hydrogen in the anode stream is lower for thick membranes compared to thin membranes even combined with a PtCo catalyst. However, this appears to be less relevant because the region where the role of the oxidation/ recombination catalyst is more important is that at low current densities.

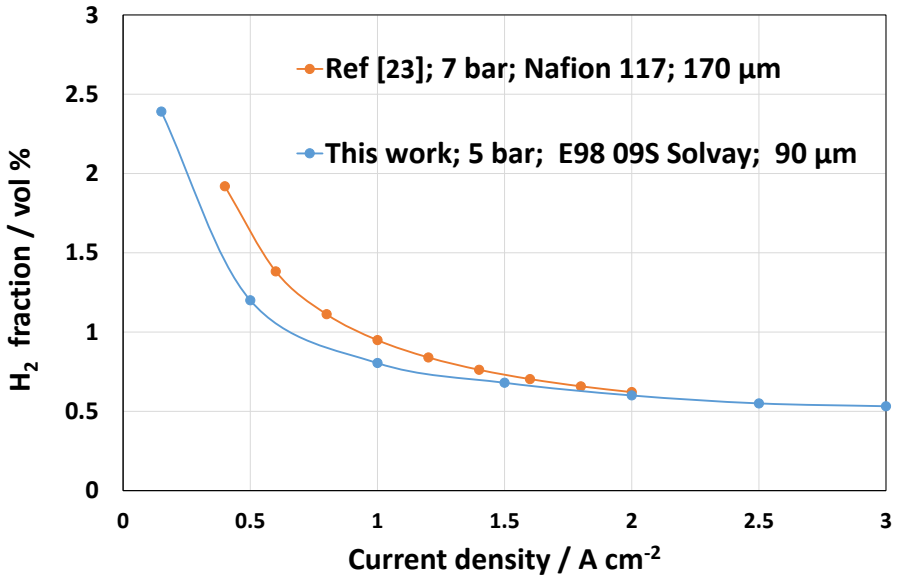

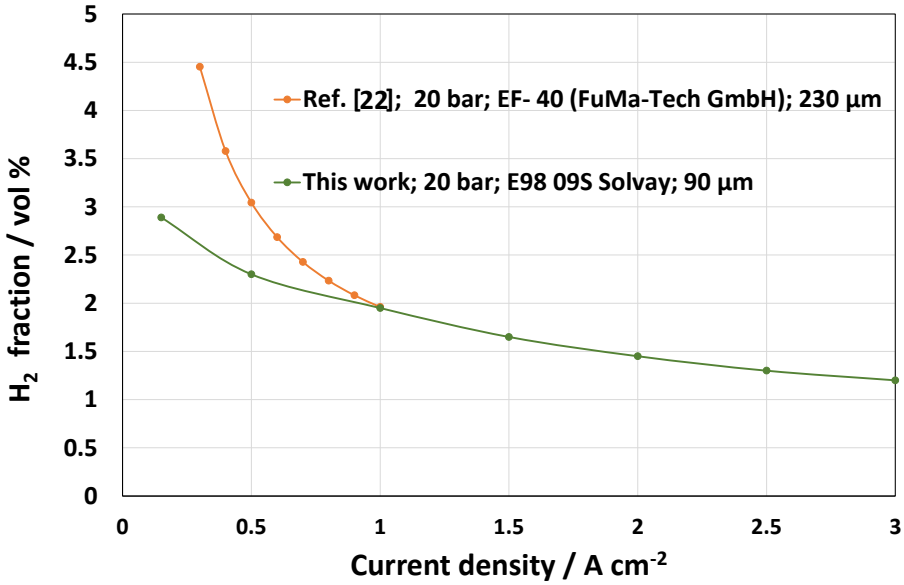

Fig. 13 Comparison of the H_2 concentration in the outlet anode stream for the present PtCo oxidation catalyst-modified MEA and the literature results for conventional MEAs based on thicker membranes.

On the other hand, one may consider the opportunity to further decreasing the thickness of the membrane in the presence of the PtCo catalyst but this may require sacrificing in part the extension of the partial load operating range compared to thick membranes. This would mean a less flexible system to cope with dynamic electricity production from renewable sources.

For the moment, the PtCo catalyst appears beneficial in terms of reduction of the hydrogen concentration in the anodic stream when it is combined with a membrane of proper thickness. The increased catalyst cost, due to the additional PtCo layer, is largely compensated by a significant increase of the hydrogen production rate (lower capital costs) at the same efficiency as consequence of the reduced ohmic losses associated to the thin membrane.

4. Conclusions

A Pt-Co alloy catalyst showed good H_2-O_2 recombination capability in the gas phase after exposure to 4% vol. H_2 in O_2; this was not the case of a PtRu alloy. According to the XPS results, the recombination performance appears to be correlated with the capability of the PtCo alloy system to keep Pt sites in a reduced oxidation state compared to other Pt catalysts. For the PtCo system, during operation in the gas phase catalytic reactor, it was observed that about 99.5% of H_2 was immediately converted to water when it was fed at 4% vol. in the oxygen stream (flammability limit).

Integration of the PtCo alloy catalyst in the membrane-electrode assembly, in particular between the membrane and the IrRuOx anode catalyst, showed also good electrochemical performance for the oxidation of the permeated hydrogen. In this case, the mechanism mainly consisted in an electrochemical oxidation of the permeated H_2 into protons that were transported back to the cathode by the electroosmotic drag. At the cathode, these ions were reduced again to molecular hydrogen. This parasitic current was not affecting much the faradaic efficiency of the system that remained larger than 99% in almost the overall range of operating current densities.

The H_2 concentration in the oxygen stream of the PEM electrolyser decreased significantly at all pressures in the presence of the PtCo catalyst. At 20 bar differential pressure, in the presence of PtCo, the hydrogen concentration in the anodic oxygen stream was well below the flammability limit also when the current density was as low as 0.15 A cm^{-2}. This corresponds to 5% partial load operation for the nominal current density of 3 A cm^{-2} for the present system compared to a conventional minimum partial load of 20% for conventional electrolysis systems. This characteristic provides better flexibility to cope with the dynamic behaviour of renewable power sources. The observed H_2 concentration in the oxygen stream for the present electrolysis system is lower than that reported in the literature for PEM electrolysis cells operating at both similar pressures and current densities in the presence of much thicker membranes-based electrolytes.

Acknowledgements

CNR-ITAE authors acknowledge the financial support from the NEPTUNE project. This project has received funding from Fuel Cells and Hydrogen 2 Joint Undertaking under grant agreement N^{o} 779540. This Joint Undertaking receives support from the European Union's Horizon 2020 research and innovation programme and Hydrogen Europe and Hydrogen Europe Research.

The authors also thank Solvay Specialty Polymers for supplying the membrane and the ionomer, ITM Power (UK) for supplying the high-pressure single cell test fixture and Mr. Giuseppe Monforte for the XPS analysis.

References

[1] S. Chu, Y.Cui , N. Liu, The path towards sustainable energy, Nat. Mater. 16 (2017) 16–22.

[2] J.J. West, S.J. Smith, R.A. Silva, V. Naik, Y. Zhang, Z. Adelman, M.M. Fry, S. Anenberg, L.W. Horowitz, J.-F. Lamarque, Co-benefits of mitigating global greenhouse gas emissions for future air quality and human health Nature Climate Change, 3 (10) (2013) 885-889.

[3] D. Shindell, G. Faluvegi, K. Seltzer, C. Shindell, Quantified, localized health benefits of accelerated carbon dioxide emissions reductions, Nature Climate Change, (2018) 1-5. Article in Press. DOI: 10.1038/s41558-018-0108-y

[4] A. Hussain, S.M. Arif, M. Aslam, Emerging renewable and sustainable energy technologies: State of the art, Renew. Sustain. Energy Rev. 71 (2017) 12-28.

[5] J. Rifkin, The Hydrogen Economy: The Creation of the Worldwide Energy Web and the Redistribution of Power on Earth, Ed. J.P. Tarcher/Penguin, 2003 ISBN 1585422541, 9781585422548.

[6] I. Hadjipaschalis, A. Poullikkas, V. Efthimiou, Overview of current and future energy storage technologies for electric power applications, Renew. Sustain. Energy Rev., 13 (2009) 1513–1522.

[7] V. R. Stamenkovic, D. Strmcnik, P. P. Lopes, N. M. Markovic, Energy and fuels from electrochemical interfaces, Nat. Mater. 16 (2017) 57–69.

[8] A.S. Aricò, S. Siracusano, N. Briguglio, V. Baglio, A. Di Blasi, V. Antonucci, Polymer electrolyte membrane water electrolysis: Status of technologies and potential applications in combination with renewable power sources, J. Appl. Electrochem. 43 (2013) 107-118.

[9] M. Balat, Potential importance of hydrogen as a future solution to environmental and transportation problems, Int. J. Hydrogen Energy, 33 (2008) pp. 4013-4029.

[10] S. Cherevko, S. Geiger, O. Kasian, N. Kulyk, J.-P. Grote, A. Savan, B.R. Shrestha, S. Merzlikin, B. Breitbach, A. Ludwig, K.J. Mayrhofer, Catal. Today 262 (2015) 170–180

[11] J.A. Turner, Sustainable Hydrogen Production, Science 305 (5686) (2004) 972-974.

[12] M.W. Kanan, D.G. Nocera, In situ formation of an oxygen-evolving catalyst in neutral water containing phosphate and Co^{2+}, Exfoliation of layered double hydroxides for enhanced oxygen evolution catalysis, Science 321 (2008) 1072-1075.

[13] F. Song, X. Hu, Exfoliation of layered double hydroxides for enhanced oxygen evolution catalysis, Nat. Commun. 5 (2014) 4477-4477

[14] M. Carmo, D.L. Fritz, J. Mergel, D. Stolten, A comprehensive review on PEM water electrolysis, Int. J. Hydrogen Energy 38 (2013) 4901-4934.

[15] V. Schröder, B. Emonts, H. Janßen, H.-P. Schulze, Explosion limits of hydrogen/oxygen mixtures at initial pressures up to 200 bar Chemical Engineering and Technology, 27 (2004) 847-851.

[16] S. Siracusano, V. Baglio, N.Van Dijk, L.Merlo, A. S. Aricò, Enhanced performance and durability of low catalyst loading PEM water electrolyser based on a short-side chain perfluorosulfonic ionomer. Appl. Energy 192 (2017) 477–489,

[17] S. Siracusano, N. Hodnik, P. Jovanovic, F. Ruiz-Zepeda, M. Šala, V. Baglio, A. S. Aricò, New insights into the stability of a high performance nanostructured catalyst for sustainable water electrolysis. Nano Energy 40 (2017) 618–632

[18] M. Bernt, H. Gasteiger, A. Influence of Ionomer Content in IrO_2/TiO_2 Electrodes on PEM Water Electrolyzer Performance, J. Electrochem. Soc. 163 (2016) F3179–F3189.

[19] S. Siracusano, S. Trocino, N. Briguglio, V. Baglio and A. S. Aricò, Electrochemical Impedance Spectroscopy as a Diagnostic Tool in Polymer Electrolyte Membrane Electrolysis, Materials, 11 (8) 1368.

[20] K. Elsøe, L. Grahl-Madsen, G. G. Scherer, J. Hjelm, M. B. Mogensen, Electrochemical Characterization of a PEMEC Using Impedance Spectroscopy. J. Electrochem. Soc. 164 (2017) F1419–F1426.

[21] S. A. Grigoriev, V.I. Porembskiy, S.V. Korobtsev, V.N. Fateev, F. Auprêtre, P.Millet, High-pressure PEM water electrolysis and corresponding safety issues, Int. J. Hydrogen Energy, 36 (2011) 2721-2728.

[22] P. Trinke, B. Bensmann, R. Hanke-Rauschenbach, Current density effect on hydrogen permeation in PEM water electrolyzers, Int. J. Hydrogen Energy, 42 (2017) 14355-4366.

[23] M. Schalenbach Erratum: pressurized PEM water electrolysis: efficiency and gas crossover. Int. J. Hydrogen Energy 2013; 38:14921-33. Int. J. Hydrogen. Energy 41 (1) (2016) 729-732.

[24] A. Brouzgou, S.Q. Song, P. Tsiakaras, Low and non-platinum electrocatalysts for PEMFCs: Current status, challenges and prospects Appl. Cat. B: Environ., 127 (2012) 371-388.

[25] H.A. Gasteiger, S.S. Kocha, B. Sompalli, F.T. Wagner, Activity benchmarks and requirements for Pt, Pt-alloy, and non-Pt oxygen reduction catalysts for PEMFCs, Appl. Cat. B: Environ., 56 (2005) 9-35.

[26] R. Owston, V. Magi, J. Abraham, Interactions of hydrogen flames with walls: Influence of wall temperature, pressure, equivalence ratio, and diluents Int. J. Hydrogen. Energy, 32 (2007) 2094-2104.

[27] D. Bessarabov, Membranes with recombination catalyst for hydrogen crossover reduction: Water electrolysis ECS Transactions, 85 (2018) 17-25.

[28] S.A. Grigoriev, P. Millet, S.V. Korobtsev, V.I. Porembskiy, M. Pepic, C. Etievant, C. Puyenchet, V.N. Fateev, Hydrogen safety aspects related to high-pressure polymer electrolyte membrane water electrolysis Int. J. Hydrogen. Energy, 34 (2009) 5986-5991.

[29] S. Siracusano, V. Baglio, S.A. Grigoriev, L. Merlo, V.N. Fateev, A.S. Aricò, The influence of iridium chemical oxidation state on the performance and durability of oxygen evolution catalysts in PEM electrolysis Journal of Power Sources, 366, (2017) 105-114.

[30] S. Siracusano, N. Van Dijk, E. Payne-Johnson, V. Baglio, A.S. Aricò, Enhanced performance and durability of low catalyst loading PEM water electrolyser based on a short-side chain perfluorosulfonic ionomer, Appl. Cat. B: Environ.164 (2015) 488–495.

[31] C. Rozain, E. Mayousse, N. Guillet, P. Millet, Influence of iridium oxide loadings on the performance of PEM water electrolysis cells: Part I-Pure IrO_2-based anodes Appl. Cat. B: Environ., 182 (2016) 153-160.

[32] S. Choe, B.-S. Lee, M.K. Cho, H.-J. Kim, D. Henkensmeier, S.J. Yoo, J.Y. Kim, S.Y. Lee, H.S. Park, J.H. Jang, Electrodeposited IrO_2/Ti electrodes as durable and cost-effective anodes in high-temperature polymer-membrane-electrolyte water electrolyzers, Appl. Cat. B: Environ., 226, (2018) 289-294.

[33] H. Yu, N. Danilovic, Y. Wang, W. Willis, A. Poozhikunnath, L. Bonville, C. Capuano, K. Ayers, R. Maric, Nano-size IrOx catalyst of high activity and stability in PEM water electrolyzer with ultra-low iridium loading Appl. Cat. B: Environ., 239 (2018) 133-146.

[34] B.-S. Lee, S.H. Ahn, H.-Y.Park, I.Choi, S.J. Yoo, H.-J.Kim, D. Henkensmeier, J.Y. Kim, S.Park, S.W. Nam, K.-Y. Lee, J.H. Jang, Development of electrodeposited IrO_2 electrodes as anodes in polymer electrolyte membrane water electrolysis Appl. Cat. B: Environ., 179 (2015) 285-291.

[35] S. Siracusano, V.Baglio, E. Moukheiber, L. Merlo, A.S.Arico, Performance of a PEM water electrolyser combining an IrRu-oxide anode electrocatalyst and a shortside chain Aquivion membrane Int. J. Hydrogen Energy, 40 (2015) 14430-14435.

[36] J. Herranz, J. Durst, E. Fabbri, A. Patru, X. Cheng, A.A. Permyakova, T.J. Schmidt, Interfacial effects on the catalysis of thehydrogen evolution, oxygen evolution and CO2-reduction reactions for (co-)electrolyzer development, Nano Energy 29 (2016) 4-28.

[37] M. Angeles Montero, J. L. Fernández, M. Rosa Gennero de Chialvo, A. C. Chialvo, Kinetic Study of the Hydrogen Oxidation Reaction on Nanostructured Iridium Electrodes in Acid Solutions J. Phys. Chem. C, , 117 (2013) 25269–25275

[38] L. Xinchun, Q. Weizhong, C. Wei, S. Congyu, S. Yongjun, Y. Xiaoqiu, Recombination of Hydrogen and Oxygen in Fluidized Bed Reactor with Different Gas Distributors, Energy Procedia Volume 29 (2012) 552-558.

[39] V. Shepelin, D. Koshmanov, E. Chepelin, Catalyst for recombination of hydrogen and oxygen in confined spaces under high concentrations of hydrogen Nuclear Technology, 178 (2012) 29-38.

[40] H. Ito, N. Miyazaki, M. Ishida, A. Nakano, Cross-permeation and consumption of hydrogen during proton exchange membrane electrolysis Int. J. Hydrogen Energy, 41 (2016) 20439-20446.

[41] D. Bessarabov, A.J. Kruger, S.M. Luopa, J. Park, A.A. Molnar, K.A. Lewinski, Gas crossover mitigation in PEM water electrolysis: Hydrogen cross-over benchmark study of 3M's Ir-NSTF based electrolysis catalyst-coated membranes ECS Transactions, 75 (2016) 1165-1173.

[42] S. Abdalla, F. Al-Marzouki, A. Obaid, Safety considerations during production and consumption of hydrogen using proton exchange membrane electrolysis, J. Renew. Sustain. Energy, 9 (2017) 013101.

[43] P. Trinke, P. Haug, J. Brauns, B. Bensmann, R. Hanke-Rauschenbach, T. Turek, Hydrogen crossover in PEM and alkalinewater electrolysis: Mechanisms, direct comparison and mitigation strategies J. Electrochem. Soc., 165 (2018) F502-F513.

[44] M. Schalenbach, A.R. Zeradjanin, O. Kasian, S. Cherevko, K.J.J. Mayrhofer, A perspective on low-temperature water electrolysis - Challenges in alkaline and acidic technology, International Journal of Electrochemical Science, 13 (2018) 1173-1226.

[45] M. Watanabe, H. Uchida, M. Emori, Analyses of self-humidification and suppression of gas crossover in Pt-dispersed polymer electrolyte membranes for fuel cells (1998) J. Electrochem. Soc., 145 (4), pp. 1137-1141.

[45] N. Mamaca, E. Mayousse, S. Arrii-Clacens, T.W. Napporn, K. Servat, N. Guillet, K.B. Kokoh, Electrochemical activity of ruthenium and iridium based catalysts for oxygen evolution reaction, Appl. Cat. B: Environ., 111-112, (2012) 376-380.

[46] M. Schalenbach, D. Stolten, High-pressure water electrolysis: Electrochemical mitigation of product gas crossover (2015) Electrochim. Acta, 156, pp. 321-327.

[47] S. Zhao, A. Stocks, B. Raimick, K. More, H. Xu, J. Electrochem. Soc., 165 (2018) F82.

[48] A.S. Aricò, Shukla, A.K. Kim, H. Park, S. Min, M. Antonucci, V. XPS study on oxidation states of Pt and its alloys with Co and Cr and its relevance to electroreduction of oxygen, Applied Surface Science, 172 (2001) 33-40.

[49] A.S. Aricò, A. Stassi, I. Gatto, G. Monforte, E. Passalacqua, V. Antonucci, Surface properties of Pt and PtCo electrocatalysts and their influence on the performance and degradation of high-temperature polymer electrolyte fuel cells Journal of Physical Chemistry C, 114 (2010) 15823-15836.

[50] S. Mukerjee, Role of Structural and Electronic Properties of Pt and Pt Alloys on Electrocatalysis of Oxygen Reduction An In Situ XANES and EXAFS Investigation J. Electrochem. Soc., 142 (1995) 1409-1422.

[51] U.A. Paulus, A. Wokaun, G.G. Scherer, T.J. Schmidt, V. Stamenkovic, N.M. Markovic, P.N. Ross, Oxygen reduction on high surface area Pt-based alloy catalysts in comparison to well defined smooth bulk alloy electrodes, Electrochim. Acta, 47 (2002) 3787-3798.

[52] N.M. Marković, H.A. Gasteiger, P.N. Ross Jr., X. Jiang, I. Villegas, M.J. Weaver, Electro-oxidation mechanisms of methanol and formic acid on Pt-Ru alloy surfaces Electrochim. Acta, 40 (1995) 91-98.

[53] A. Stassi, I. Gatto, V. Baglio, E. Passalacqua, A.S. Aricò, Oxide-supported PtCo alloy catalyst for intermediate temperature polymer electrolyte fuel cells, Appl. Cat. B: Environ., 142-143 (2013) 15-24.

[54] P. Lettenmeier, R. Wang, R. Abouatallah, S. Helmly, T. Morawietz, R. Hiesgen, S. Kolb, F. Burggraf, J. Kallo, A. S. Gago, K. A. Friedrich, Durable Membrane Electrode Assemblies for Proton Exchange Membrane Electrolyzer Systems Operating at High Current Densities, Electrochim. Acta 210 (2016) 502–511.

[55] S. Hu, G. Goenaga, C. Melton, T.A. Zawodzinski, D. Mukherjee, PtCo/CoOx nanocomposites: Bifunctional electrocatalysts for oxygen reduction and evolution reactions synthesized via tandem laser ablation synthesis in solution-galvanic replacement reactions, Appl. Cat. B: Environ., 182 (2016) 286-296.

[56] K. Jayasayee, J.A.R.V. Veen, T.G. Manivasagam, S. Celebi, E.J.M. Hensen, F.A. de Bruijn, Oxygen reduction reaction (ORR) activity and durability of carbon supported PtM (Co, Ni, Cu) alloys: Influence of particle size and non-noble metals, Appl. Cat. B: Environ., 111-112 (2012) 515-526.

[57] P. Hernández-Fernández, S. Rojas, P. Ocón, J.L.G. de la Fuente, P. Terreros, M.A. Peña, J.L. García-Fierro, An opening route to the design of cathode materials for fuel cells based on PtCo nanoparticles Appl. Cat. B: Environ., 77 (2007) 19-28.

[58] C. Kathleen Taylor, Determination of ruthenium surface areas by hydrogen and oxygen chemisorption, Journal of Catalysis, 38 (1975) 299-306.

[59] A.S. Aricò, S. Srinivasan, V. Antonucci, DMFCs: From fundamental aspects to technology development, Fuel Cells 1 (2001) 133-161.

[60] A.S. Arico, G. Monforte, E. Modica, P.L. Antonucci, V. Antonucci, Investigation of unsupported Pt-Ru catalysts for high temperature methanol electro-oxidation Electrochem. Commun., 2 (2000) 466-470.

[61] A. Marshall, B. Børresen, G. Hagen, M. Tsypkin, R. Tunold, Energy 32 (2007) 431-436.

[62] I. Katsounaros, S. Cherevko, A.R. Zeradjanin, K.J.J. Mayrhofer, Angew. Chem. Int. Ed. 53 (2014) 102-121.

[63] S. Song, H. Zhang, X. Ma, Z. Shao, R.T. Baker, B. Yi, Int. J. Hydrogen Energy 33 (2008) 4955-4961.

[64] J.C. Cruz, V. Baglio, S. Siracusano, R. Ornelas, L. Ortiz-Frade, L.G. Arriaga, V. Antonucci, A.S. Aricò, Nanosized IrO_2 electrocatalysts for oxygen evolution reaction in an SPE electrolyzer J. Nanopart. Res., 13 (2011) 1639-1646.

[65] J. Xu, D. Aili, Q. Li, E. Christensen, J.O. Jensen, W. Zhang, M.K. Hansen, G. Liu, X. Wang, N.J. Bjerrum, Energy Environ. Sci. 7 (2014) 820-830.

[66] D. Zhang K. Zeng,Evaluating the Behavior of Electrolytic Gas Bubbles and Their Effect on the Cell Voltage in Alkaline Water Electrolysis Ind. Eng. Chem. Res., 51 (2012) 13825–13832.

[67] P. Millet, A. Ranjbari, F. De Guglielmo, S.A. Grigoriev, F. Auprêtre, Cell failure mechanisms in PEM water electrolyzers Int. J. Hydrogen Energy, 37 (2012) 17478-17487.

[68] P. Trinke, B. Bensmann, R. Hanke-Rauschenbach, Experimental evidence of increasing oxygen crossover with increasing current density during PEM water electrolysis, Electrochem. Commun., 82 (2017) 98-102.

[69] B. Bensmann, R. Hanke-Rauschenbach, K. Sundmacher, In-situ measurement of hydrogen crossover in polymer electrolyte membrane water electrolysis Int. J. Hydrogen Energy, 39 (2014) 49-53.

[70] A.H. Reksten, H. Thuv, F. Seland, S. Sunde, Journal of Electroanal. Chem. The oxygen evolution reaction mechanism at $IrxRu_{1-x}O_2$ powders produced by hydrolysis synthesis 819 (2018) 547-561

Figure1

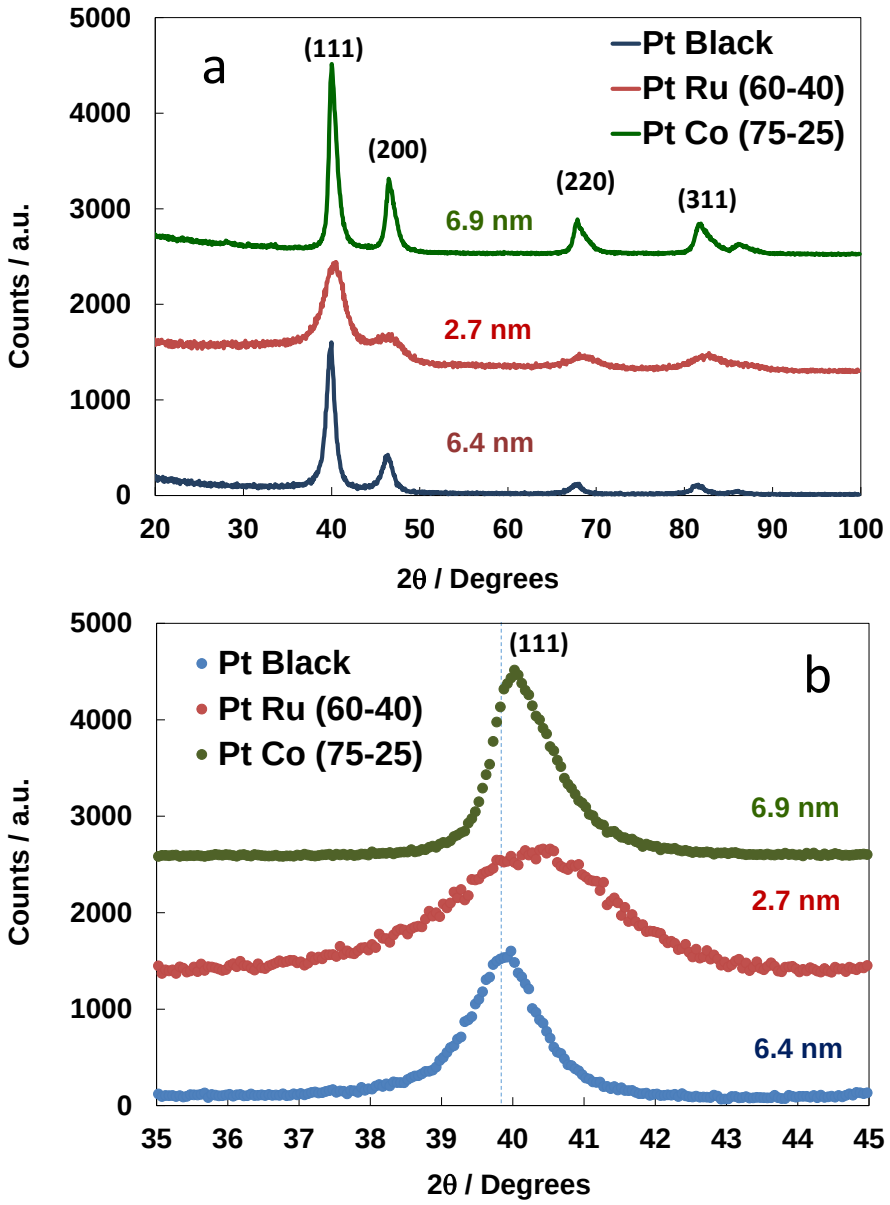

Fig. 1 X-ray diffraction patterns of the recombination/hydrogen electro-oxidation catalysts; a) full range; b) magnification of the Pt (111) reflection region.

Figure2

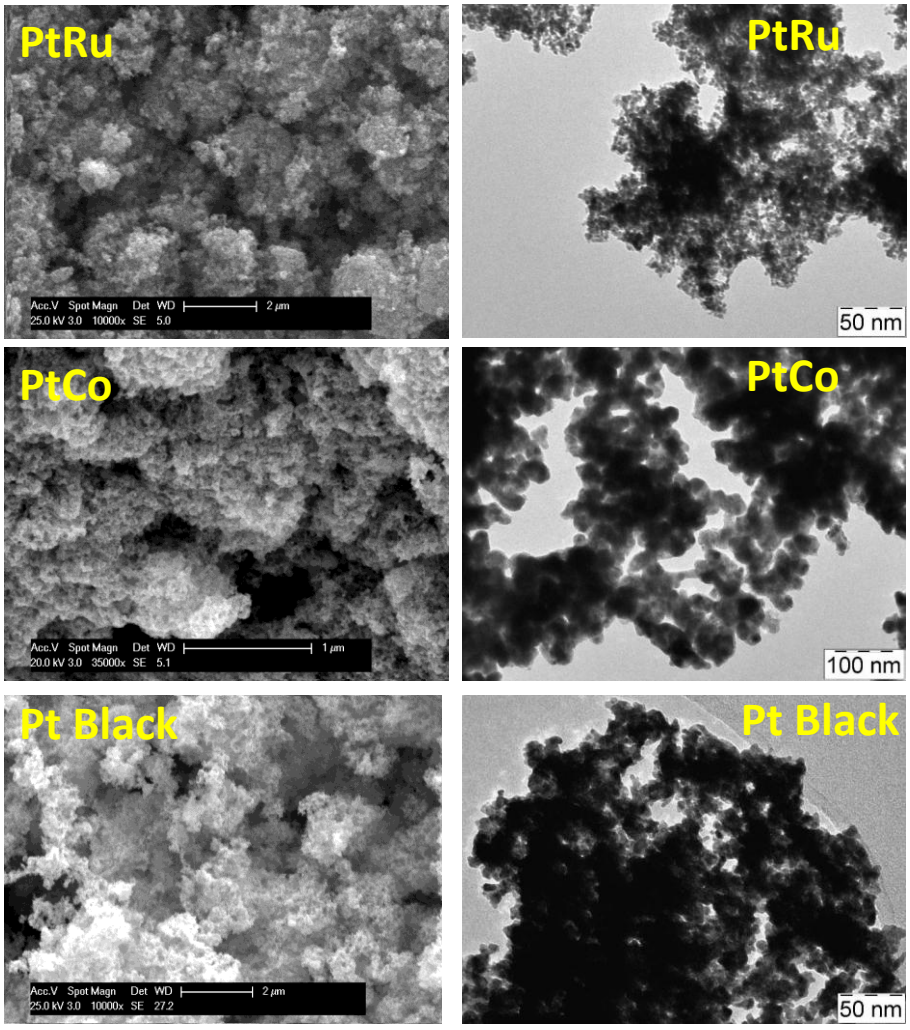

Fig. 2 Scanning (left) and transmission (right) electron micrographs of the recombination / hydrogen electro-oxidation catalysts

Figure3

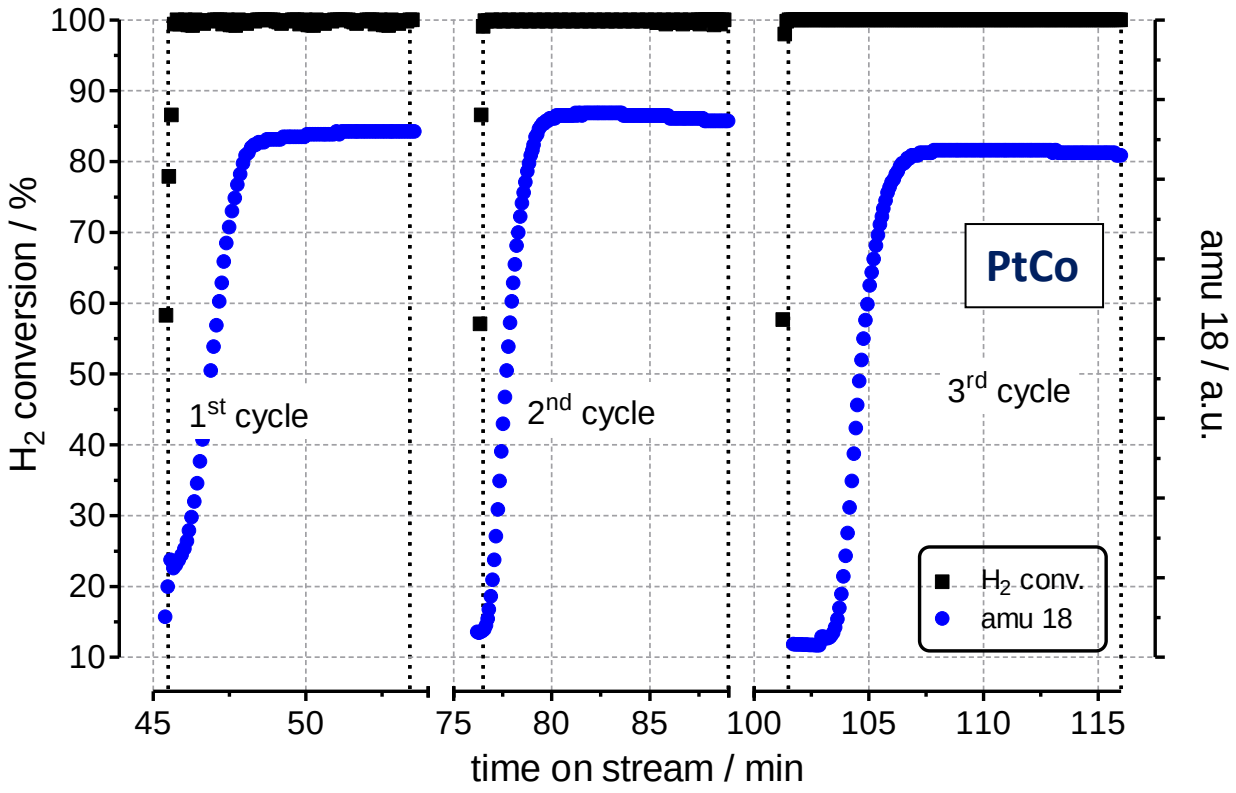

Fig. 3 Hydrogen conversion and water formation (H_2O = 18 amu-atomic mass unit) as a function of time at PtCo in a packed-bed catalytic reactor upon 4% vol. H_2 feed in a pure oxygen stream (three cycles). In each cycle, the catalyst was exposed to pure oxygen before feeding the 4% vol. H_2 – 96 % vol. O_2 mixture.

Figure4

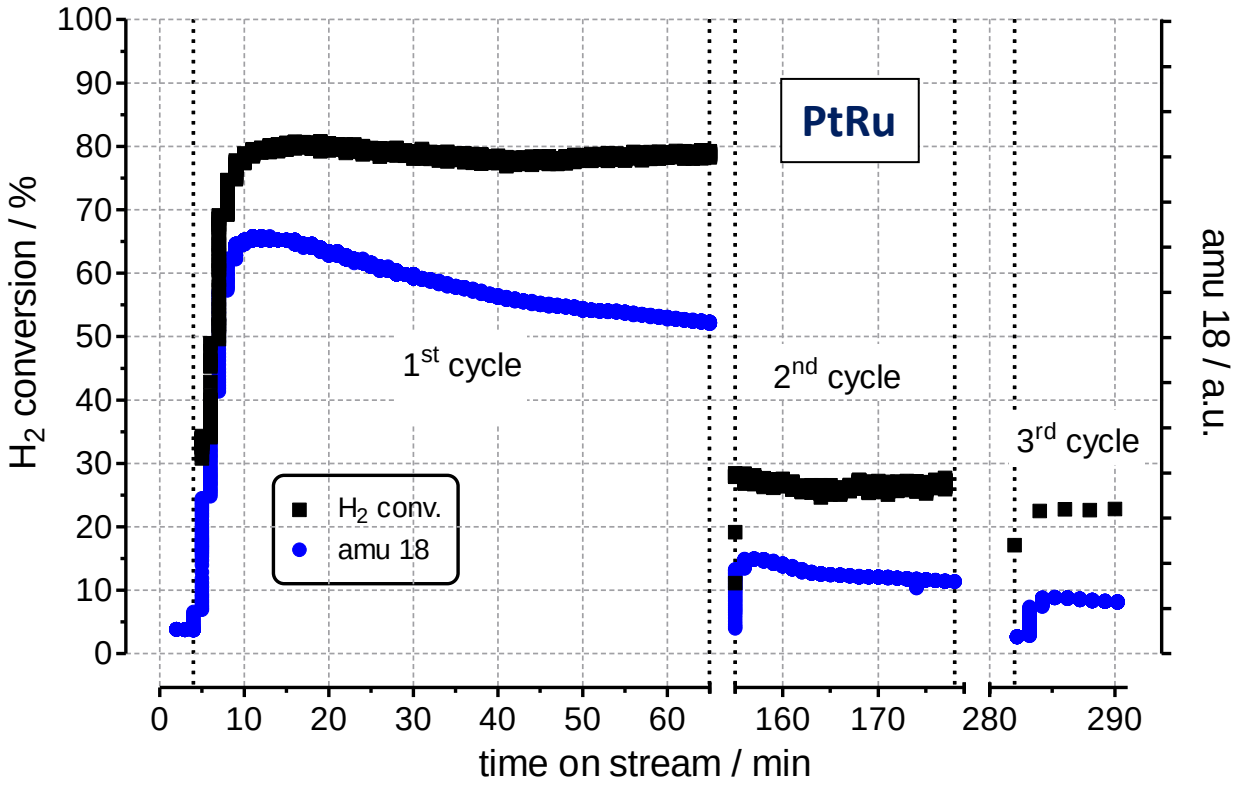

Fig. 4 Hydrogen conversion and water formation (H_2O = 18 amu-atomic mass unit) as a function of time at PtRu in a packed-bed catalytic reactor upon 4% vol. H_2 feed in a pure oxygen stream (three cycles). In each cycle, the catalyst was exposed to pure oxygen before feeding the 4 % vol. H_2 – 96 % vol. O_2 mixture.

Figure5

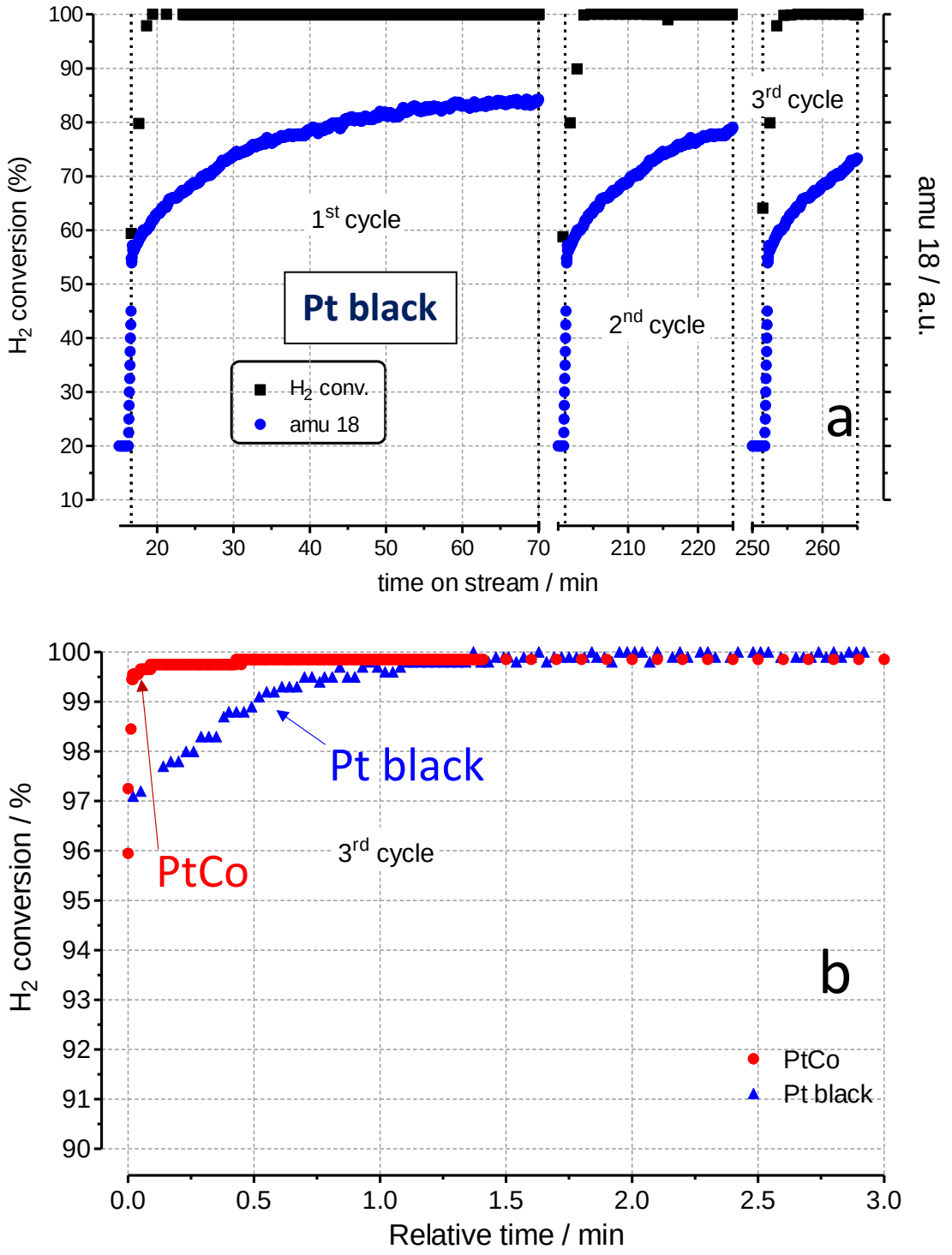

Fig. 5 a) Hydrogen conversion and water formation (H_2O = 18 amu-atomic mass unit) as a function of time at Pt black in a packed-bed catalytic reactor upon 4% vol. H_2 feed in a pure oxygen stream. In each cycle, the catalyst was exposed to pure oxygen before feeding the 4 % vol. H_2 – 96 % vol. O_2 mixture. b) Comparison of H_2 conversion response versus time for PtCo and Pt black catalytic systems after three cycles.

Figure6

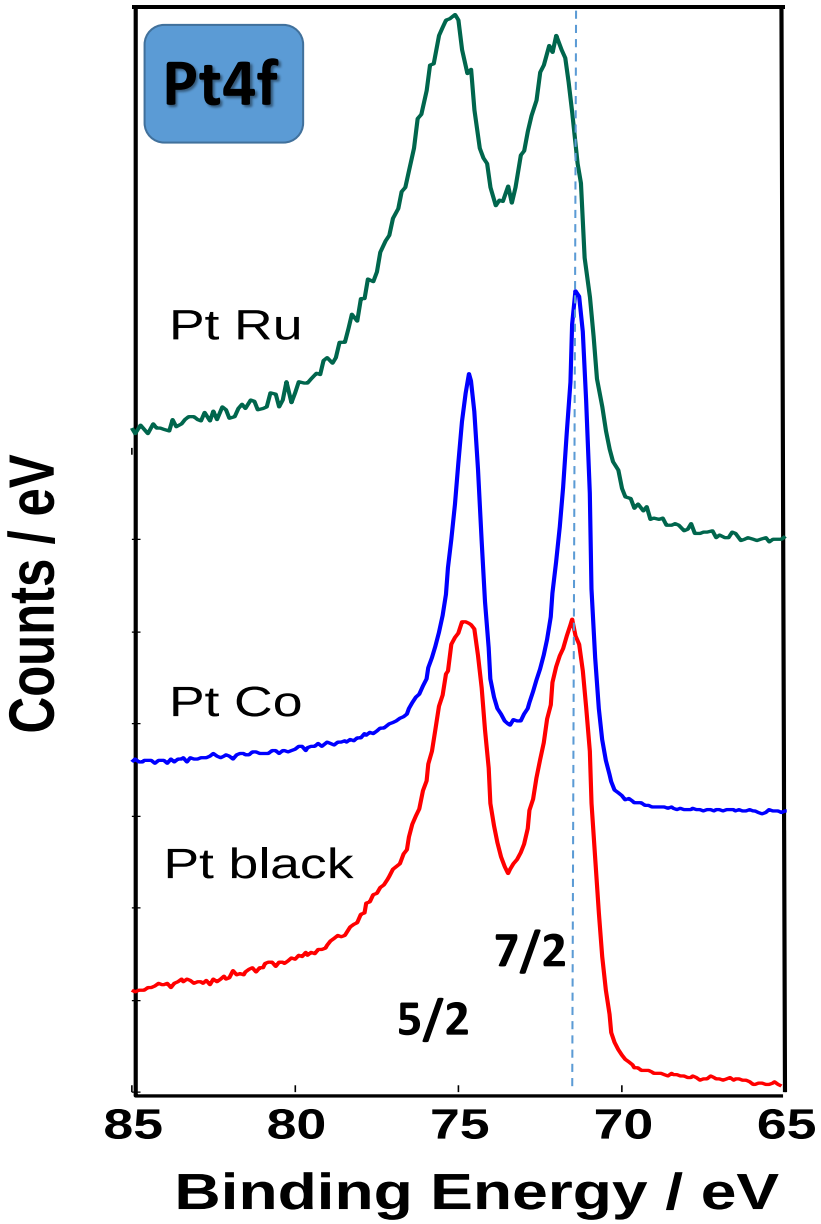

Fig. 6 High resolution X-ray photoelectron spectra of the Pt4f region of the recombination/hydrogen electro-oxidation catalysts

Figure7

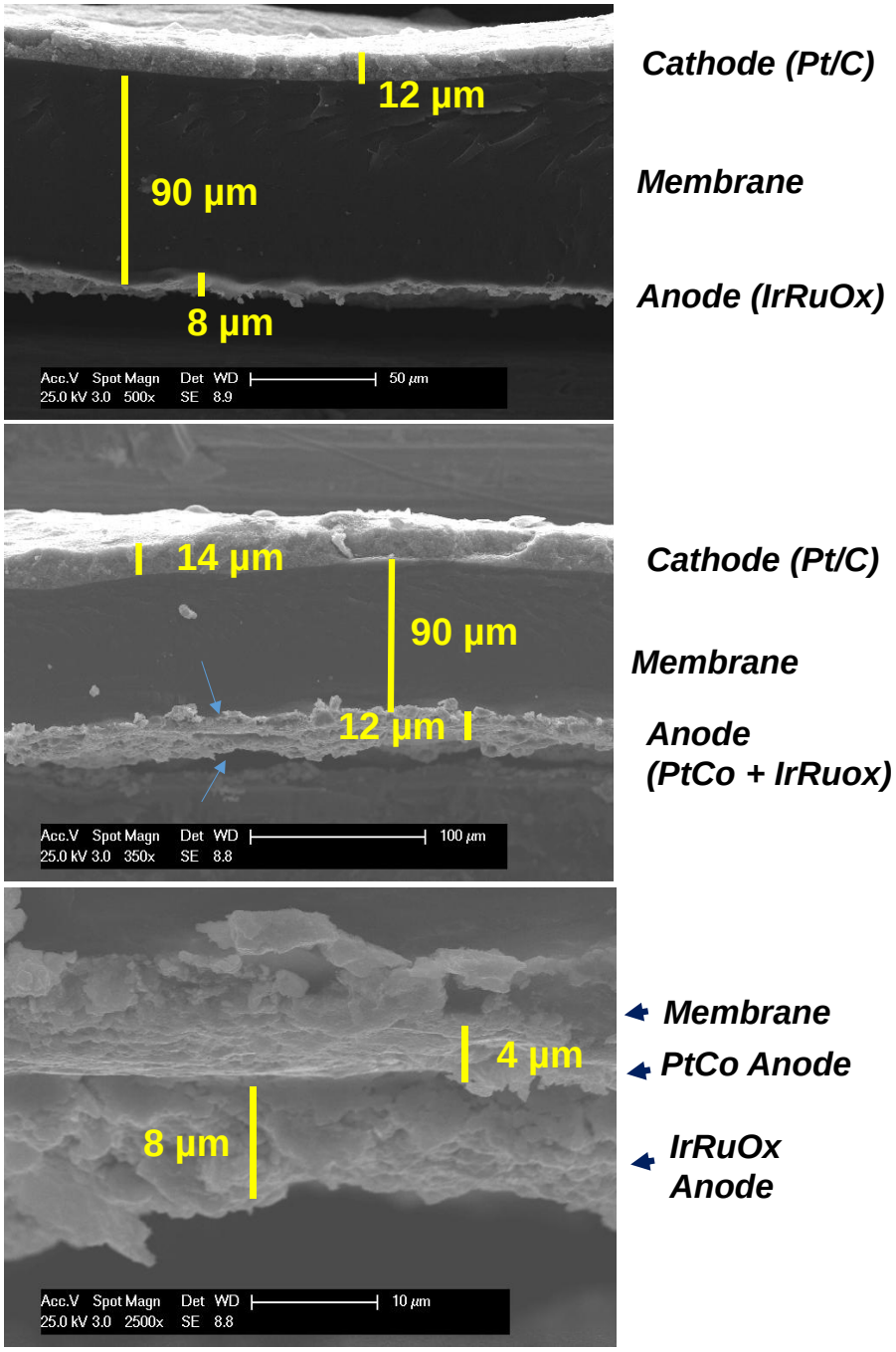

Fig. 7 Scanning electron micrographs of the MEAs (a) without and (b) with the PtCo hydrogen electro-oxidation catalysts

Figure8

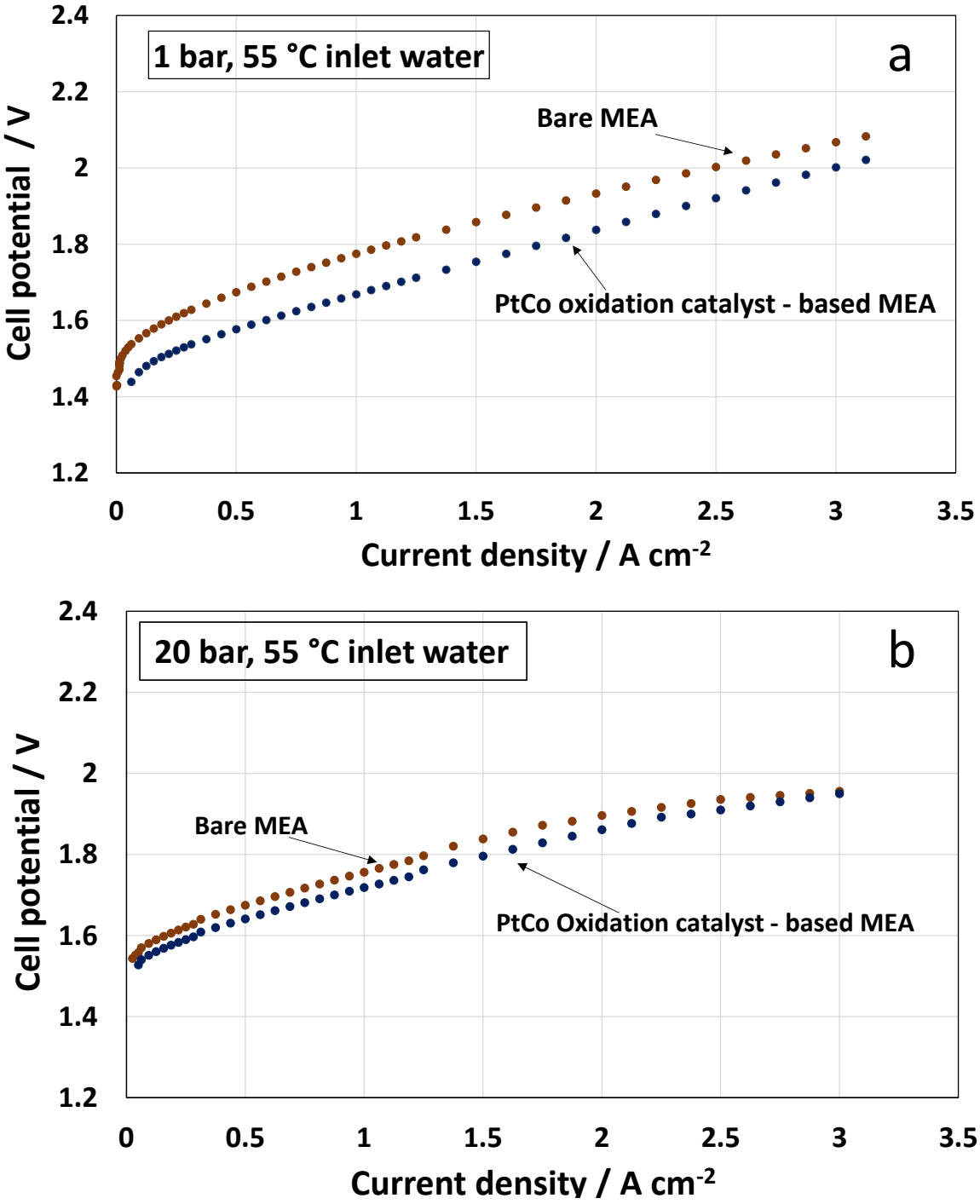

Fig. 8 Electrolysis polarization curves for the bare MEA and the MEA containing the PtCo oxidation catalyst at (a) 1 bar and (b) 20 bar differential pressure, at a constant water inlet temperature of 55 °C.

Figure9

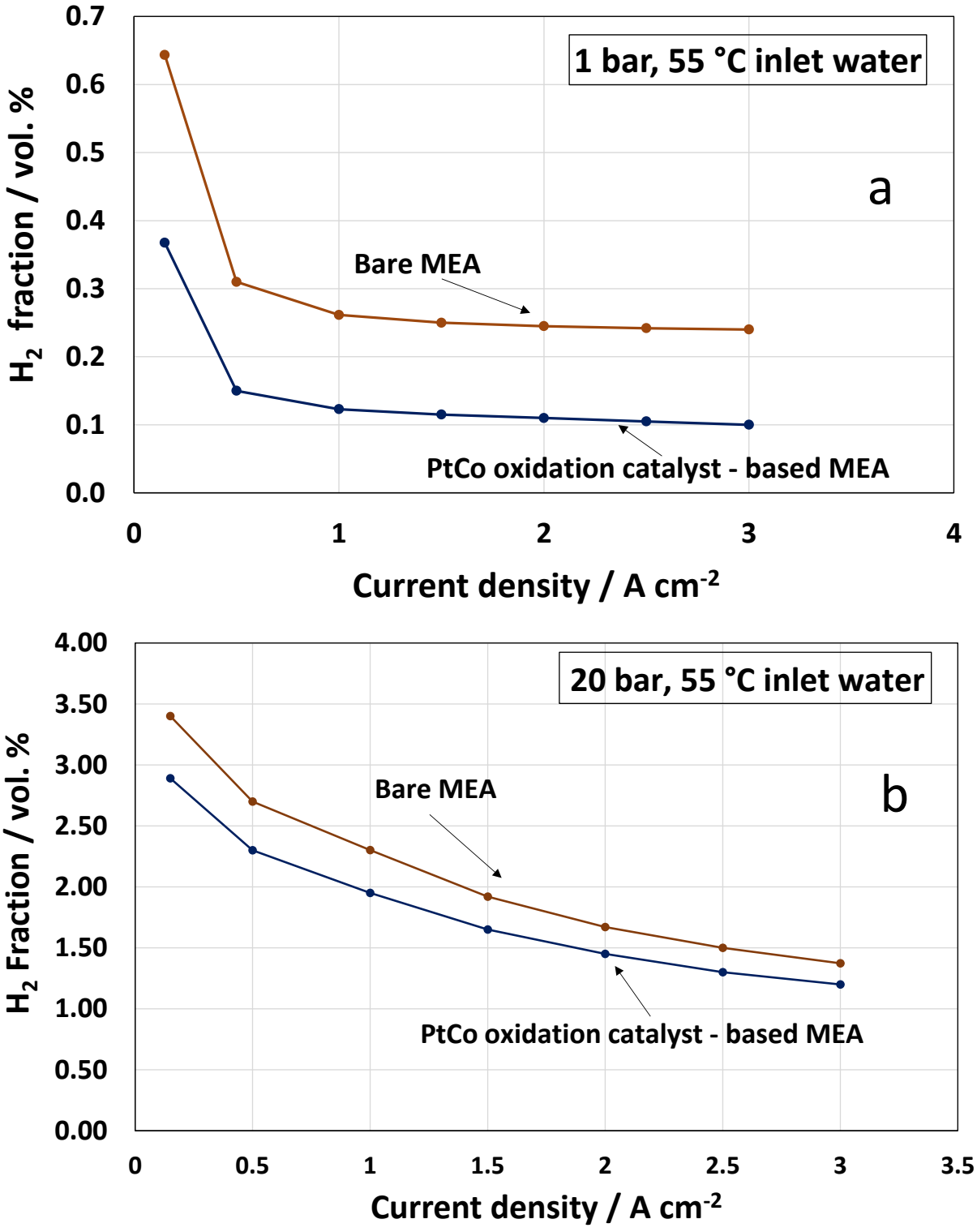

Fig. 9 Hydrogen fraction in the outlet anode stream at various current densities for the bare MEA and the MEA containing the PtCo oxidation catalyst at (a) 1 bar and (b) 20 bar differential pressure, at a constant water inlet temperature of 55 °C.

Figure10

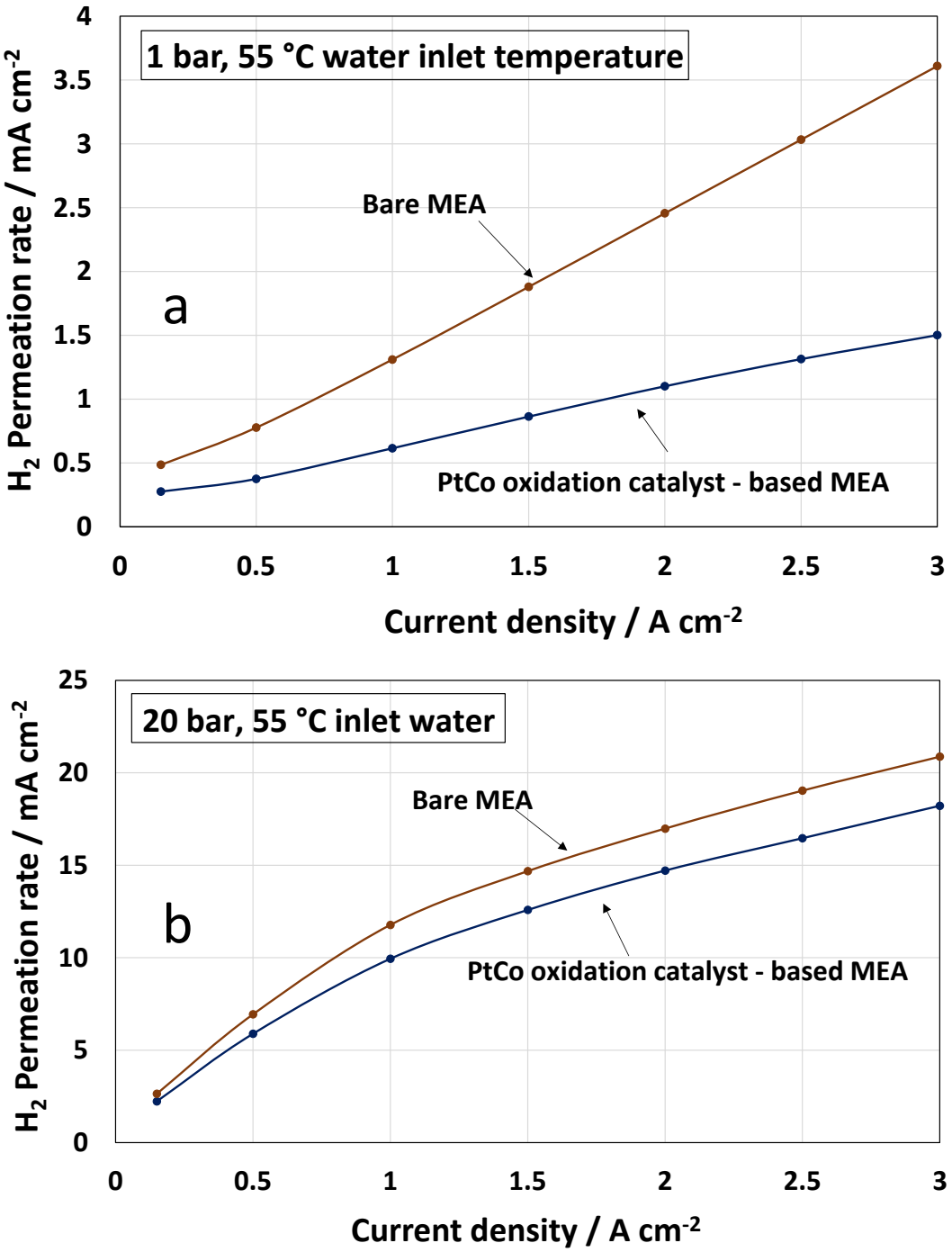

Fig. 10 Equivalent current density for the hydrogen fraction in the outlet anode stream at various electrolysis current densities for the bare MEA and the MEA containing the PtCo oxidation catalyst at (a) 1 bar and (b) 20 bar differential pressure, at a constant water inlet temperature of 55 °C.

Figure11

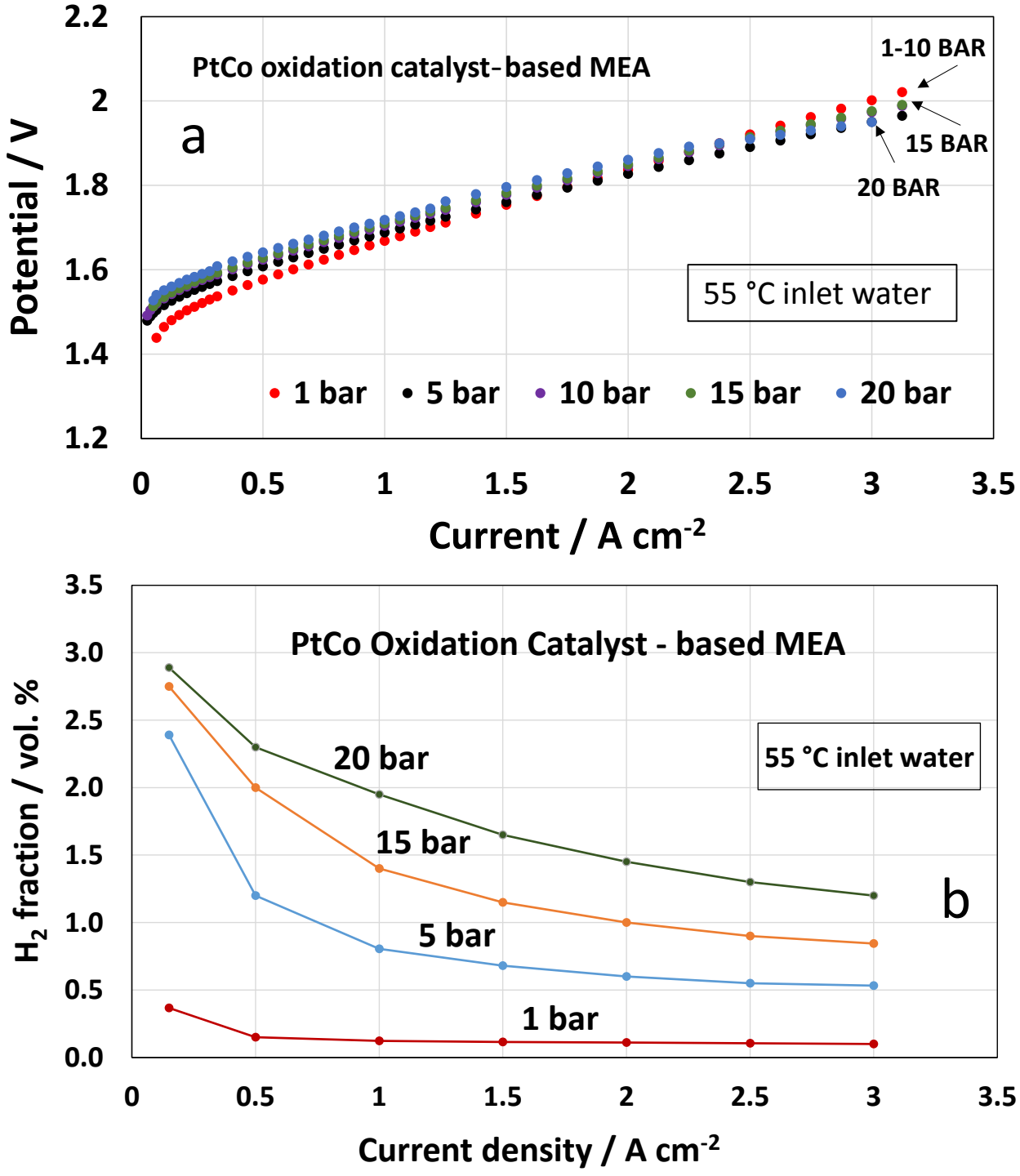

Fig. 11 Polarisation curves (a) and hydrogen fraction in the outlet anode stream (b), at different pressures, for the MEA containing the PtCo oxidation catalyst, at a constant water inlet temperature of 55 °C.

Figure12

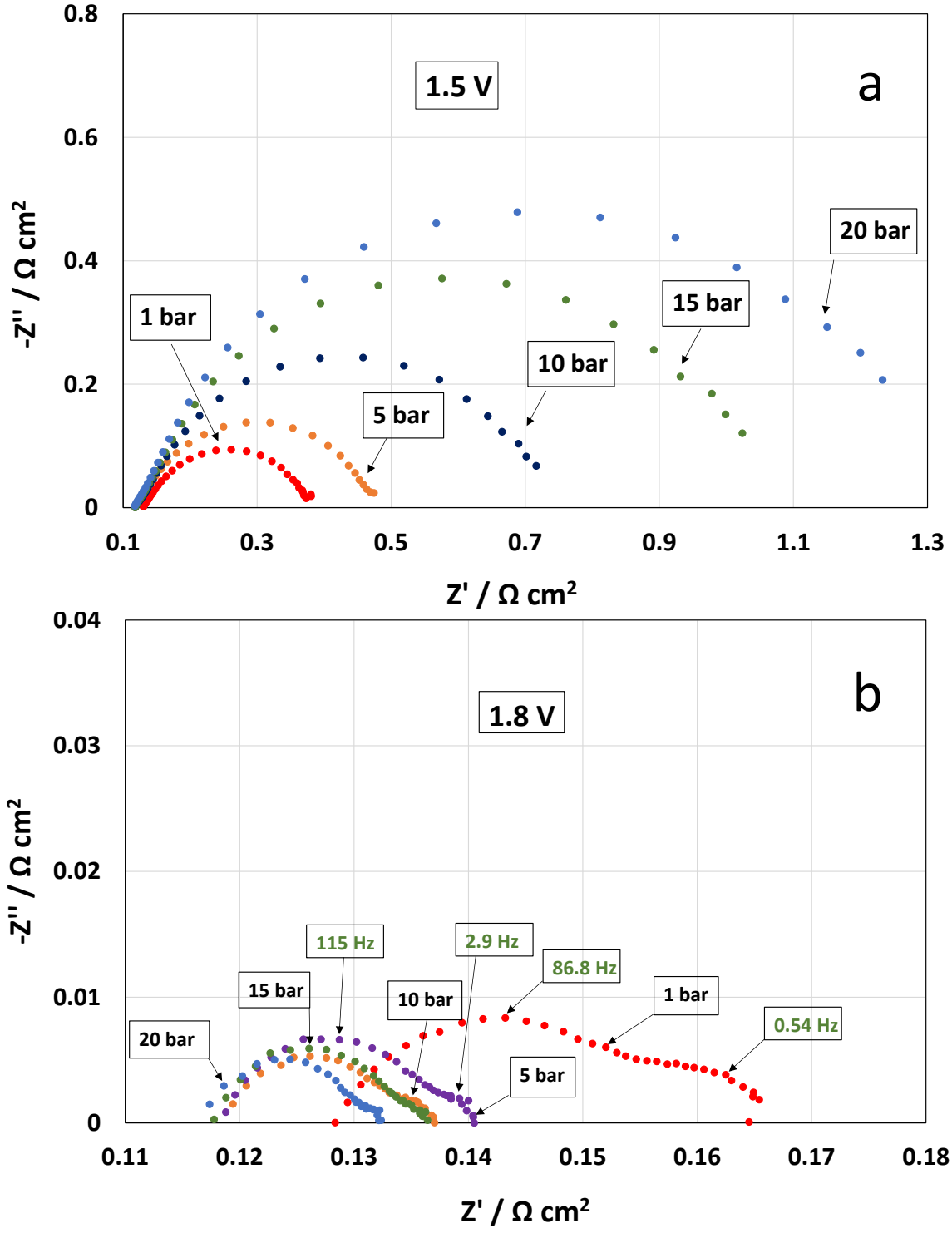

Fig. 12 Electrochemical impedance spectra, at 1.5 V (a) and 1.8 V (b), at different pressures, for the MEA containing the PtCo oxidation catalyst, at a constant water inlet temperature of 55 °C.

Figure13

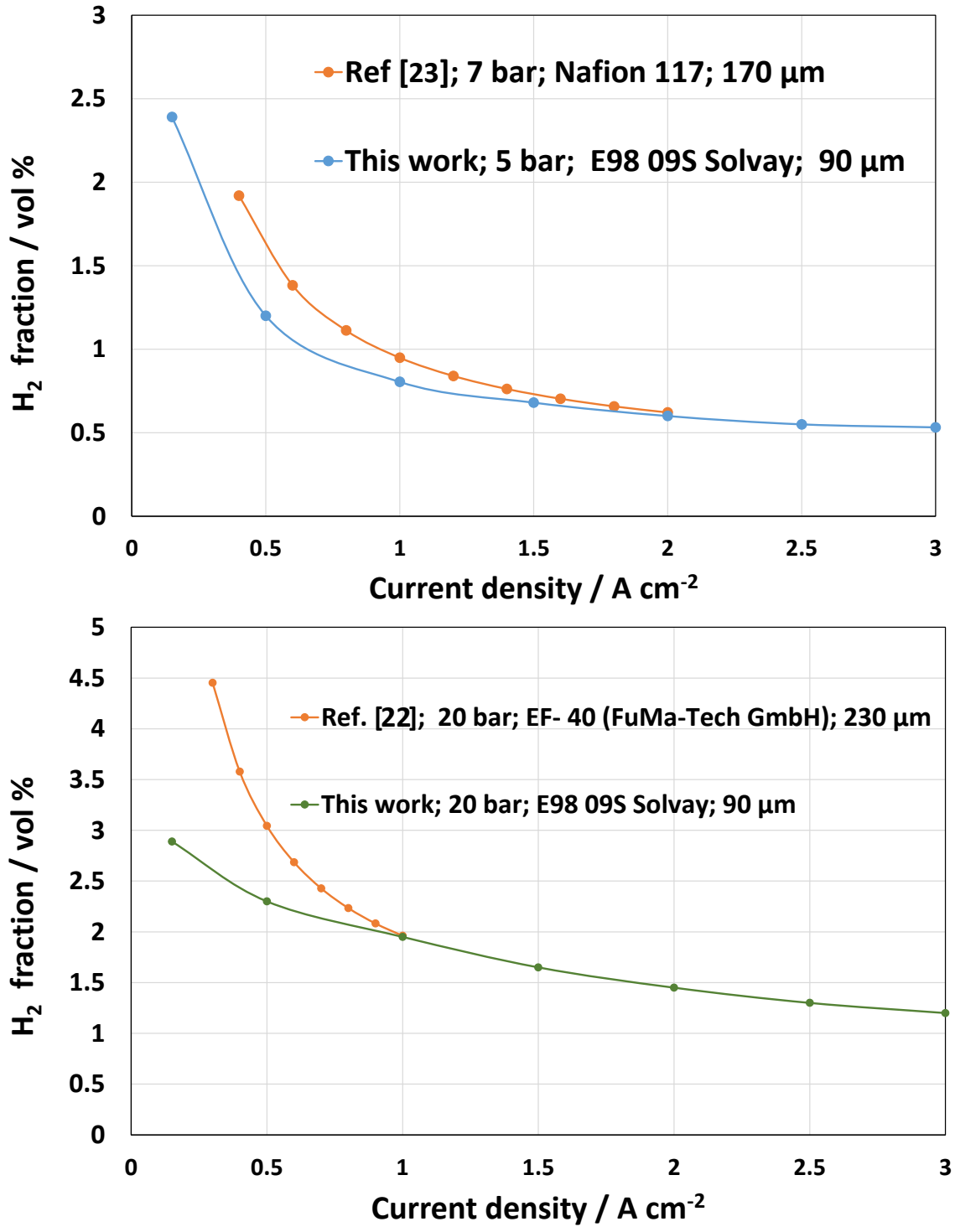

Fig. 13 Comparison of the H_2 concentration in the outlet anode stream for the present PtCo oxidation catalyst-modified MEA and the literature results for conventional MEAs based on thicker membranes.

*Graphical Abstract

Graphical Abstract

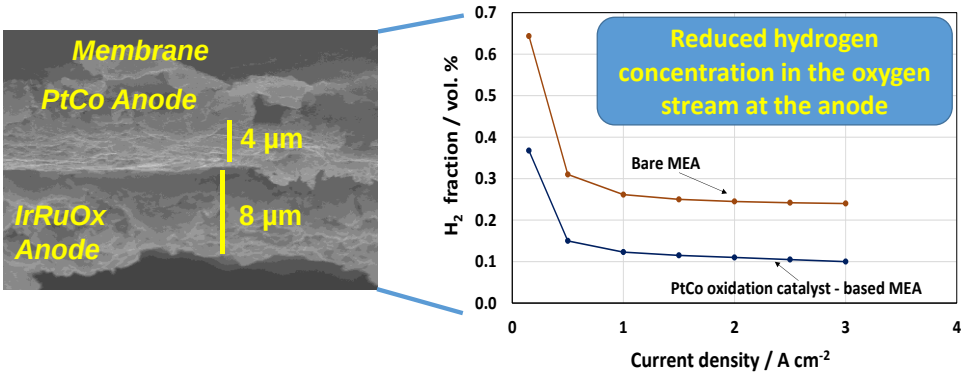

Highlights

PtCo alloy is demonstrated as dynamic and efficient H_2-O_2 recombination catalyst.

Recombination performance correlates with the Pt metallic state on the surface.

80% electrolysis efficiency at 3 A cm^{-2} is obtained with a PtCo/IrRuOx anode at 55°C.

Under electrolysis, hydrogen oxidation at PtCo reduces its fraction in the O_2 stream.

H_2 oxidation at PtCo reduces the flammability occurrence at partial loads at 20 bar.

Supplementary Material

Click here to download Supplementary Material: SUPPLEMENTARY DATA Recombination catalyst 20-10-2018.docx